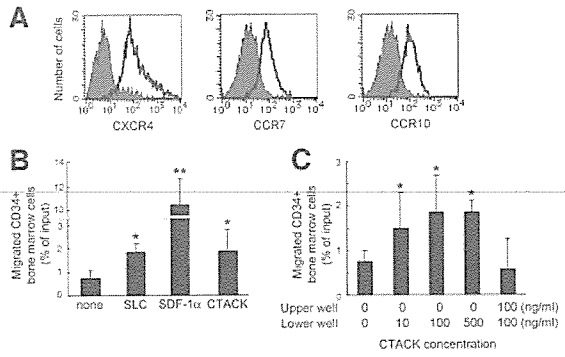

Figure 2. CCR10, a receptor for CTACK, was expressed in $CD34^+$ bone marrow (BM) cells and these $CD34^+$ BM cells migrated in response to CTACK in vitro. **(A):** Expression of CXCR4, a receptor for SDF-1α; CCR7, a receptor for SLC; and CCR10 on $CD34^+$ BM cells was analyzed by flow cytometry. Shown are the staining with a specific antibody for each chemokine receptor (solid line) and the background staining with the nonspecific immunoglobulin antibody (negative isotype-matched control; shaded profile) by the gated $CD34^+$ population. $CD34^+$ BM cells expressed CXCR4 (97.4%), CCR7 (12.9%), and CCR10 (19.1%). **(B, C):** Chemotaxis assays were undertaken in vitro. Isolated $CD34^+$ BM cells purified by fluorescence-activated cell sorting were added to the upper well of a 3-μm-pore Transwell. Recombinant SLC, SDF-1α, or CTACK was added to the upper and/or lower plate. $CD34^+$ BM cell migration rates increased in response to medium containing recombinant SLC, SDF-1α, or CTACK (100 ng/ml) ($* p < .05$, $** p < .001$) versus medium alone ($n = 4$) **(B)**. CTACK (0–500 ng/ml) induced $CD34^+$ BM cell migration in dose-dependent manner ($n = 4$) ($* p < .05$) **(C)**. SDF-1α and SLC also induced in dose-dependent manner (data not shown). Abbreviations: CTACK, cutaneous T-cell attracting chemokine; SDF-1α, stromal cell-derived factor-1α; SLC, secondary lymphoid tissue chemokine.

CTACK Treatment Specifically Led to Accumulations of BMDKs in Wounded Skin

To assess the ability of chemokines in keratinocyte precursor cell recruitment in vivo, we injected these chemokines to the periphery of wounded skin in enhanced GFP transgenic transplanted mice. The number of GFP-positive BMDKs in the epidermis was calculated ($n = 5$ mice in each group). Although SDF-1α and SLC failed to influence the number of BMDKs compared with the controls, CTACK significantly increased the number of BMDKs in wounded skin (Fig. 3A). Next, to clarify whether this increase of $CD34^+$ BM cells could enhance the overall number of BMDKs, we attempted to increase the levels of $CD34^+$ BM cells in peripheral blood by means of cytokine mobilization using G-CSF (five mice) or $CD34^+$ cell adoptive transfer (five mice). Increased numbers of $CD34^+$ BM cells in peripheral blood significantly enhanced the number of BMDKs in wounded skin in each group. In addition, CTACK treatment in this group significantly increased the number of BMDKs by approximately fivefold compared with the controls in each group (Fig. 3A). Furthermore, intradermal injection of CTACK neutralizing antibody inhibited this BMDK migration in a dose-dependent manner (five mice) (Fig. 3B).

CTACK Treatment Accelerated BMDK-Induced Wound Healing

We determined that CTACK was capable of inducing additional BMDKs that could participate in the host skin wound response. Surprisingly, intradermal injection of CTACK significantly accelerated wound closure (six mice) (Fig. 4A, 4B). We speculated that this effect was mediated by increases in BMDK. However, there are several possible reasons why intradermal injection of CTACK might accelerate wound repair. This could represent increased angiogenesis, keratinocyte proliferation, or keratinocyte migration during wound healing. Therefore, the following additional experiments were performed. We examined whether CTACK induced angiogenesis in wound healing. Three days after skin wounding, when the greatest number of new capillaries were formed [20], the number of dermal capillaries was calculated on two sections from each mouse (five mice per treatment group) and on an identical wound site section with or without CTACK injection (PBS vehicle control). CTACK had no effect on angiogenesis in wounded skin (Fig. 4C). Next, to determine whether CTACK induced keratinocyte proliferation, we measured proliferation rates in vitro. CTACK had no effect on the proliferation of the keratinocytes (six mice) (Fig. 4D). It has previously been reported that CCR10 is expressed on only skin-homing memory T cells. In our study, we confirmed that keratinocytes and fibroblasts in normal and wounded skin did not express CCR10 (data not shown). Finally, to determine whether CTACK induced keratinocyte migration, we undertook a keratinocyte migration assay in vitro. CTACK had no effect on keratinocyte migration. These results indicate that intradermal injection of CTACK accelerated wound healing without influencing angiogenesis, keratinocyte proliferation, or migration.

Discussion

We have shown that CTACK is a major regulator of keratinocyte precursor cell migration from the BM to the skin. In this study, BM-derived cells were able to transdifferentiate into keratinocytes at the sites of skin wounds. Furthermore, we have shown that CTACK is specifically expressed in wounded skin and that $CD34^+$ BM cells express CCR10, the main CTACK receptor. Although the numbers of BMDKs in untreated skin wounds are extremely low, a combination of treatments to increase the number of peripheral blood $CD34^+$ BM-derived cells, together with intradermal injection of CTACK into the wounded skin periphery, resulted in a 10-fold increase of BMDK. Furthermore, an increase in circulating $CD34^+$ BM cells enhanced the number of BMDKs, suggesting that a significant number of $CD34^+$ cells are included in the BMDK precursor population. Intradermal injection of CTACK significantly accelerated wound closure via increased rates of BMDK accumulation. We concluded that small populations of the progenitor cells coexpressing CD34 and CCR10 exist, that a subset of these cells migrated to the epidermis in response to CTACK, and that these cells play important roles in skin wound healing and repair.

Tissue repair and regeneration after injury is thought to involve the selective recruitment of circulating or resident stem cell populations. Chemokine/chemokine receptor interactions are expected to contribute to these mechanisms of stem cell plasticity. However, only one chemokine/chemokine receptor interaction, the SDF-1α/CXCR4 interaction, has thus far been reported. The SDF-1α/CXCR4 interaction has been identified as a factor causing hematopoietic stem cell mobilization [19]; however, other tissue cells are recruited from the BM by this

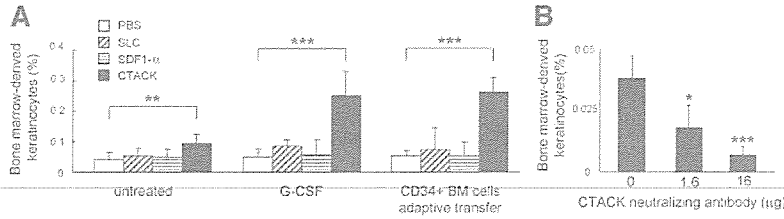

Figure 3. CTACK specifically accumulated bone marrow-derived keratinocytes (BMDKs) in wounded skin. **(A):** The number of BMDKs was quantified as a percentage of the total number of keratinocytes in wounded skin from untreated mice or those treated with G-CSF for cytokine mobilization or those that received $CD34^+$ BM cell adoptive transfer. SLC, SDF-1α, or CTACK (1 μg in 30 μl) was intradermally injected into the periphery of wounded skin (five mice in each group). CTACK significantly accumulated large numbers of BMDKs as compared with SLC, SDF-1α, and PBS (** $p < .01$). Furthermore, the number of BMDKs increased in mice treated with G-CSF for cytokine mobilization or those that received $CD34^+$ BM cell adoptive transfer (*** $p < .005$). **(B):** CTACK neutralizing antibody (0–16 μg in 120 μl) was injected to the periphery of wounded skin. The numbers of BMDKs were decreased by CTACK neutralizing antibody in dose-dependent manner (five mice) (* $p < .05$, *** $p < .005$). Abbreviations: BM, bone marrow; CTACK, cutaneous T-cell attracting chemokine; G-CSF, granulocyte colony stimulating factor; PBS, phosphate-buffered saline; SDF-1α, stromal cell-derived factor-1α; SLC, secondary lymphoid tissue chemokine.

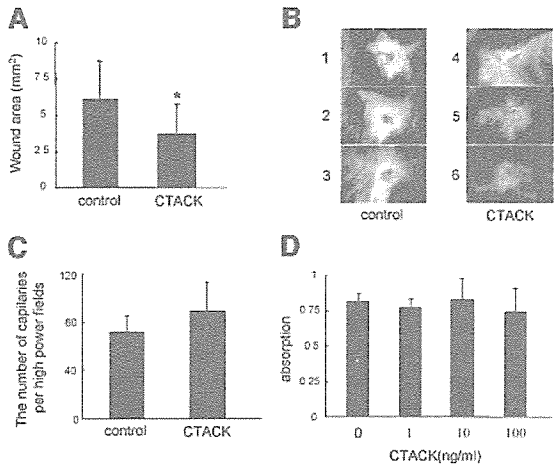

Figure 4. Increased bone marrow-derived keratinocytes (BMDKs) by CTACK accelerated wound closure without angiogenesis or keratinocyte proliferation. **(A, B):** Wound size was measured at 10 days after wounding and subsequent CTACK treatment (total 3 μg in 100 μl) or PBS (100 μl) as control (six mice in each group). Full-thickness cutaneous wounds were made and subsequently monitored daily. Intradermal injection of CTACK significantly accelerated wound closure (* $p < .05$) **(A)**. Representative images at 10 days after wounding of wounds treated with PBS (as control) (mice 1–3) or CTACK (mice 4–6) **(B)**. **(C):** The numbers of capillaries in the dermis treated by CTACK (1 μg in 30 μl) or PBS (30 μl) (as control vehicle) at 3 days after wounding were quantified. There was no statistical difference between CTACK and control (two sections each of five mice). **(D):** Keratinocytes were cultured with or without CTACK (0–100 ng/ml) for 72 hours, and viable cells were determined by proliferation assay. There was no statistical difference in proliferation of keratinocytes between the two treatment groups (nine mice). Abbreviations: CTACK, cutaneous T-cell attracting chemokine; PBS, phosphate-buffered saline.

interaction, including myocytes [21] and neural cells [22]. In addition, SDF-1α and CXCR4 are widely expressed on various cell types, and SDF-1α/CXCR4 interactions play an important role in several developmental and regenerative phenomena, such as cardiogenesis [21], neovascularization [23], hematopoiesis [19], and hepatic development [24]. Furthermore, wounding stimulated the engraftment of BM cells into the skin and induced BM-derived cells to incorporate into and differentiate into nonhematopoietic skin structures [25]. Given that it is unlikely that this receptor interaction is involved in many cell functions, organ-specific chemokine/chemokine receptor interactions are predicted. Indeed, we have demonstrated that the CTACK/CCR10 interaction is involved in skin wound healing. A strategy to detect further tissue-specific chemokines expressed in injured tissue would further benefit future organ-specific BM stem cell enrichment and recruitment.

Several studies have indicated that BM-derived cells have the ability to effect tissue regeneration in protein-deficient mouse models. Mice with damaged liver function caused by a fumarylacetoacetate hydrolase deficiency recovered after normal mouse-derived hematopoietic stem cell transplantation, in which mouse BM cells transdifferentiated into hepatocytes [26]. BM-derived cells may prove beneficial for protein-deficient disease therapy. In the study, the increase in BM-derived cells might further enhance the rate of damaged tissue recovery in wild-type mice. This suggests that cells derived from circulating stem cells are more effective at enlisting host regenerative mechanisms than resident tissue cells, indicating a promising therapeutic strategy for damaged tissues. Our results provide direct evidence that tissue-specific BM precursor cells are recruited with the help of tissue-specific chemokine/chemokine receptor interactions.

ACKNOWLEDGMENTS

This work was supported in part by grants-in-aid for Scientific Research (number 133,57008 to H.S. and number 157,90563 to R.A.) and the Project for Realization of Regenerative Medicine (to H.S.) from the Ministry of Education, Science, Sports, and Culture of Japan, and Health and Labor Sciences Research Grants (numbers H13-Measures for Intractable Disease-02 and H16-Measures for Intractable Disease-02 to H.S.) from the Ministry of Health, Labor, and Welfare of Japan. We thank Ayumi Honda for excellent technical assistance.

DISCLOSURES

The authors indicate no potential conflicts of interest.

REFERENCES

1 Jackson KA, Majka SM, Wang H et al. Regeneration of ischemic cardiac muscle and vascular endothelium by adult stem cells. J Clin Invest 2001;107:1395–1402.

2 Orlic D, Kajstura J, Chimenti S et al. Bone marrow cells regenerate infarcted myocardium. Nature 2001;410:701–705.

3 LaBarge MA, Blau HM. Biological progression from adult bone marrow to mononucleate muscle stem cell to multinucleate muscle fiber in response to injury. Cell 2002;111:589–601.

4 Harris RG, Herzog EL, Bruscia EM et al. Lack of a fusion requirement for development of bone marrow-derived epithelia. Science 2004;305:90–93.

5 Brittan M, Braun KM, Reynolds LE et al. Bone marrow cells engraft within the epidermis and proliferate in vivo with no evidence of cell fusion. J Pathol 2005;205:1–13.

6 Houghton J, Stoicov C, Nomura S et al. Gastric Cancer Originating from Bone Marrow-Derived Cells. Science 2004;306:1568–1571.

7 Borue X, Lee S, Grove J et al. Bone marrow-derived cells contribute to epithelial engraftment during wound healing. Am J Pathol 2004;165:1767–1772.

8 Kollet O, Shivtiel S, Chen YQ et al. HGF, SDF-1, and MMP-9 are involved in stress-induced human $CD34^+$ stem cell recruitment to the liver. J Clin Invest 2003;112:160–169.

9 Kocher AA, Schuster MD, Szabolcs MJ et al. Neovascularization of ischemic myocardium by human bone-marrow-derived angioblasts prevents cardiomyocyte apoptosis, reduces remodeling and improves cardiac function. Nat Med 2001;7:430–436.

10 Peled A, Petit I, Kollet O et al. Dependence of human stem cell engraftment and repopulation of NOD/SCID mice on CXCR4. Science 1999; 283:845–848.

11 Peled A, Grabovsky V, Habler L et al. The chemokine SDF-1 stimulates integrin-mediated arrest of CD34(+) cells on vascular endothelium under shear flow. J Clin Invest 1999;104:1199–1211.

12 Abe R, Shimizu T, Sugawara H et al. Regulation of human melanoma growth and metastasis by AGE-AGE receptor interactions. J Invest Dermatol 2004;122:461–467.

13 Boniface K, Bernard F-X, Garcia M et al. IL-22 inhibits epidermal differentiation and induces proinflammatory gene expression and migration of human keratinocytes. J Immunol 2005 2005;174:3695–3702.

14 Morales J, Homey B, Vicari AP et al. CTACK, a skin-associated chemokine that preferentially attracts skin-homing memory T cells. Proc Natl Acad Sci U S A 1999;96:14470–14475.

15 Homey B, Alenius H, Muller A et al. CCL27-CCR10 interactions regulate T cell-mediated skin inflammation. Nat Med 2002;8:157–165.

16 Reiss Y, Proudfoot AE, Power CA et al. CC chemokine receptor (CCR)4 and the CCR10 ligand cutaneous T cell-attracting chemokine (CTACK) in lymphocyte trafficking to inflamed skin. J Exp Med 2001;194:1541–1547.

17 Dreyfus PA, Chretien F, Chazaud B et al. Adult bone marrow-derived stem cells in muscle connective tissue and satellite cell niches. Am J Pathol 2004;164:773–779.

18 Goolsby J, Marty MC, Heletz D et al. Hematopoietic progenitors express neural genes. Proc Natl Acad Sci U S A 2003;100:14926–14931.

19 Wright DE, Bowman EP, Wagers AJ et al. Hematopoietic stem cells are uniquely selective in their migratory response to chemokines. J Exp Med 2002;195:1145–1154.

20 Tonnesen MG, Feng X, Clark RA. Angiogenesis in wound healing. J Investig Dermatol Symp Proc 2000;5:40–46.

21 Askari AT, Unzek S, Popovic ZB et al. Effect of stromal-cell-derived factor 1 on stem-cell homing and tissue regeneration in ischaemic cardiomyopathy. Lancet 2003;362:697–703.

22 Imitola J, Raddassi K, Park KI et al. Directed migration of neural stem cells to sites of CNS injury by the stromal cell-derived factor 1alpha/CXC chemokine receptor 4 pathway. Proc Natl Acad Sci U S A 2004; 101:18117–18122.

23 Yamaguchi J, Kusano KF, Masuo O et al. Stromal cell-derived factor-1 effects on ex vivo expanded endothelial progenitor cell recruitment for ischemic neovascularization. Circulation 2003;107:1322–1328.

24 Lagasse E, Connors H, Al-Dhalimy M et al. Purified hematopoietic stem cells can differentiate into hepatocytes in vivo. Nat Med 2000;6:1229.

25 Badiavas EV, Abedi M, Butmarc J et al. Participation of bone marrow derived cells in cutaneous wound healing. J Cell Physiol 2003;196:245–250.

26 Jang YY, Collector MI, Baylin SB et al. Hematopoietic stem cells convert into liver cells within days without fusion. Nat Cell Biol 2004; 6:532–539.

ORIGINAL ARTICLE

Targeted Skipping of a Single Exon Harboring a Premature Termination Codon Mutation: Implications and Potential for Gene Correction Therapy for Selective Dystrophic Epidermolysis Bullosa Patients

Maki Goto[1], Daisuke Sawamura[1], Wataru Nishie[1], Kaori Sakai[1], James R. McMillan[1], Masashi Akiyama[1] and Hiroshi Shimizu[1]

This study examined the feasibility of antisense oligoribonucleotide (AON) therapy for dystrophic epidermolysis bullosa (DEB). AON was designed to induce skipping of a targeted exon containing a premature termination codon mutation, resulting in restoration of the open reading frame. We targeted exon 70 of *COL7A1*, as a recurrent mutation 5818delC in Japanese DEB patients was localized to exon 70. We found that one AON induced effective skipping of normal exon 70 containing 16 amino acids. Attachment and migration analyses showed that recombinant collagen without contribution of exon 70 was similar in effect to normal type VII collagen. Next, we synthesized mutation-specific AON by deleting cytosine at 5818. Introduction of this AON into DEB keratinocytes harboring 5818delC showed that the AON induced skipping of exon 70 in the abnormal 5818delC allele. Furthermore, 6.2% of DEB keratinocytes started to express type VII collagen *in vitro* after application of the mutation-specific AON. Injection of the AON into rat model grafted with DEB keratinocytes and fibroblasts induced a low amount of type VII collagen expression. We conclude that skipping of targeted exons using mutation-specific AON may show potential for future gene therapy for DEB patients.

Journal of Investigative Dermatology (2006) **126,** 2614–2620. doi:10.1038/sj.jid.5700435; published online 15 June 2006

INTRODUCTION

The transfer of normal genes into somatic cells is one strategy to treat patients with genetic diseases. However, this strategy still encounters problems including efficacy of gene transfer rate and practical clinical safety. Thus, other strategies, including pharmacological therapy or gene correction, are receiving increasing attention.

Recently, studies of muscular dystrophy have demonstrated the feasibility of modulating intron–exon splicing using antisense oligoribonucleotides (AONs), which may induce exon skipping, resulting in slightly shorter, but in-frame, mRNA transcripts (Mann *et al.*, 2001; Lu *et al.*, 2003). In muscular dystrophy caused by mutations in the dystrophin gene, shorter transcripts found in patients with milder phenotypes have a significantly longer life expectancy when compared to the patients with a complete loss of dystrophin expression (Monaco *et al.*, 1988; England *et al.*, 1990). These observations have led to the idea of using AON to skip abnormal, mutated exons to restore the open reading frame and convert a severe phenotype into a milder form (Mann *et al.*, 2001; Lu *et al.*, 2003). The mechanism of exon skipping is based upon AON, small synthetic RNA molecules that are designed to bind to specific sequences within the pre-mRNA (Mayeda *et al.*, 1990; Galderisi *et al.*, 1999).

Dystrophic epidermolysis bullosa (DEB) is clinically characterized by mucocutaneous blistering in response to minor trauma, followed by scarring and nail dystrophy, and patients generally exhibit tissue separation beneath the lamina densa of the epidermal basement membrane where anchoring fibrils are present in normal skin but structurally compromised in DEB (Fine *et al.*, 2000). DEB is caused by mutations in the *COL7A1* gene encoding type VII collagen, the major component of anchoring fibrils (Uitto *et al.*, 1995; Fine *et al.*, 2000). Several methods have achieved transfer of normal *COL7A1* into the patients' skin (Chen *et al.*, 2002; Ortiz-Urda *et al.*, 2002; Goto *et al.*, 2006), but this has never yet been extended to patients in clinical practice.

Previous report demonstrated an interesting DEB case whose manifestation was milder than expected from mutations in genomic DNA (McGrath *et al.*, 1999). Further mRNA analysis revealed that the mutation led to skipping of that single exon and subsequent maintenance of the open reading

[1]*Department of Dermatology, Hokkaido University Graduate School of Medicine, Sapporo, Japan*

Correspondence: Dr Daisuke Sawamura, Department of Dermatology, Hokkaido University Graduate School of Medicine, N15 W7, Sapporo 060-8638, Japan. E-mail: smartdai@med.hokudai.ac.jp

Abbreviations: AON, antisense oligoribonucleotide; DEB, dystrophic epidermolysis bullosa; HS-RDEB, Hallopeau–Siemens recessive DEB; RT-PCR, reverse transcriptase-PCR

Received 2 February 2006; revised 20 March 2006; accepted 4 April 2006; published online 15 June 2006

frame. In addition, missense mutations are known to provide unexpected *COL7A1* splicing outcomes (Wessagowit *et al.*, 2005). The *COL7A1* mutations causing single exon skipping resulted in milder cases than the predicted Hallopeau–Siemens recessive DEB phenotype (HS-RDEB) with nonsense mutations (Terracina *et al.*, 1998).

In this study, we have examined the feasibility of using AON in targeted exon skipping to modulate *COL7A1* splicing in such a manner that the translational open reading frame can be restored in keratinocytes from DEB patients.

RESULTS

Detection of exon 70 skipping in cultured keratinocytes

We targeted exon 70 for AON therapy as the recurrent premature termination codon mutation 5818delC in DEB patients was localized to exon 70 (Tamai *et al.*, 1999; Sawamura *et al.*, 2005). We synthesized two potential AONs, h70AON1 and h70AON2, which comprised full-length phosphorothioate backbone and HPLC-purified 2′-*O*-methyl-modified ribose molecules (Figure 1a). To evaluate the effects of h70AON1 and h70AON2 on *COL7A1* skipping of normal exon 70, we introduced them to HaCaT keratinocytes or normal human epidermal keratinocytes, and amplified *COL7A1* cDNA by reverse transcriptase-PCR (RT-PCR) with the forward primer on the border of exons 65 and 66, and a reverse primer on exon 72 (66–72 primer set). The h70AON1 samples showed a single 347 bp band. In the h70AON2 experiment, the samples showed a strong upper 347 bp band, whereas the lower 299 bp band was apparent (Figure 1b). Sequence analysis revealed that the upper 347 bp band consisted of exons 66, 67, 68, 69, 70, 71, and 72, whereas a lack of exon 70 was found in the lower 299 bp band. To semiquantify the amount of the lower and upper bands, we subcloned the PCR product to the TA cloning vector. The rate of the lower band to the upper band was expressed as the exon skipping rate. The result showed that the rates in samples of HaCaT cells and normal human keratinocytes were 18.2 and 28.1%, respectively. Each value represents the mean ± SD of four samples.

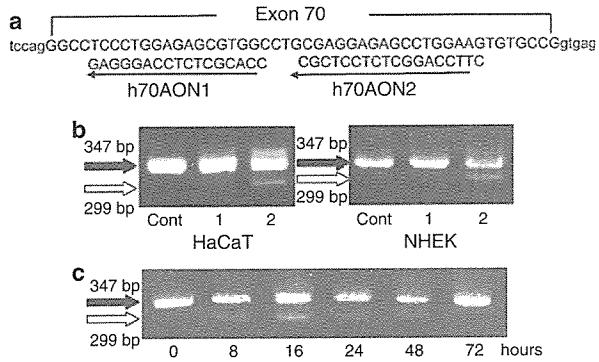

Figure 1. **Detection of exon 70 skipping in cultured keratinocytes.** The recurrent premature termination codon mutation 5818delC in DEB patients was localized to exon 70. We introduced h70AON1 and h70AON2 into HaCaT keratinocytes or normal human keratinocytes (NHEK), and amplified *COL7A1* cDNA by RT-PCR with the 66–72 primer set. (**a**) Sequences of h70AON1 and 2 are shown. (**b**) The h70AON1 samples (1) showed a single 347 bp band containing exon 70 (black arrow). The h70AON2 samples (2) showed an upper strong 347 bp band with exon 70 (black arrow), whereas the weaker lower 299 bp band without exon 70 (white arrow) was apparent. Only the 347 bp band was found in control samples without AON treatment (Cont). (**c**) We performed a time-course experiment, in which *COL7A1* expression in cultured HaCaT cells was examined 8, 16, 24, 48, and 72 hours after h70AON2 transfer. We found the highest expression of the 299 bp band at the 16 hours after AON transfer although the effect of AON was totally extinct 72 hours after the transfer.

These results indicate that h70AON2 could induce skipping of exon 70. We simultaneously performed a time-course experiment, in which *COL7A1* expression in cultured HaCaT cells was examined 8, 16, 24, 48, and 72 hours after h70AON2 transfer. We found the highest expression of the 299 bp band at 16hours after AON transfer, although the effect of AON was totally extinct 72 hours after the transfer (Figure 1c). We obtained the samples 16 hours after transfer of h70AON2 for further experiments.

Detection of exon 70 skipping *in vivo*

To simulate AON therapy in clinical practice, we transplanted human skin onto a nude rat and then injected 30 μg of h70AON2 to the graft. Saline was injected in a control. After 16 hours, the skin biopsies were taken from the injected site and were subjected to RT-PCR analysis. RT-PCR with the 66–72 primer set amplified a 347 bp strong band containing exon 70 and a weak signal of 299 bp band without exon 70 from the treated sample, whereas the control sample showed 347 bp band alone (Figure 2). We also applied 0.3 or 3 μg of h70AON2 to the graft, resulting in no signal of 299 bp band (data not shown). TA cloning of the 30 μg h70AON2 samples showed that the proportion of the lower band to the upper bands was 12.2%. To verify exon 70 skipping, we synthesized a 70Δ primer set with a forward primer on border of exons 63 and 64, and reversel primer on the border of exons 69 and 71. RT-PCR amplification with the 70Δ primer set detected a 305 bp band in only the AON-treated samples, which were indicative of exon skipping of 70 (Figure 2).

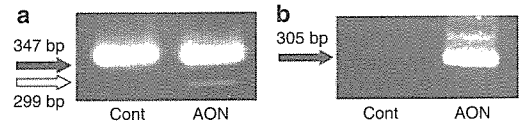

Figure 2. **Detection of exon 70 skipping *in vivo*.** We transplanted human skin to a nude rat and then injected 30 μg of h70AON2 AON into the graft. After 16 hours, the skin biopsies were taken from the injected site and were subjected to RT-PCR analysis. (**a**) RT-PCR with the 66–72 primer set amplified a 347 bp strong band (black arrow) containing exon 70 and a weaker signal of 299 bp band (white arrow) without exon 70 from the (AON)-treated sample, whereas the control sample showed a 347 bp band alone (Cont). (**b**) RT-PCR amplification with the 70Δ primer set detected a 305 bp band only in AON-treated samples. The AON lane seemed to have the higher molecular weight band in addition to the 305 bp *COL7A1* band. However, subcloning of PCR product to a TA cloning vector (Invitrogen, Carlsbad, CA) could not detect the corresponding *COL7A1* cDNA and we thought it to be a PCR artifact.

Assays for type VII collagen without exon 70

There is a possibility that the deletion of 16 amino acids, which are encoded by exon 70, may abolish some of the functions of type VII collagen. Therefore, we prepared retrovirus vector containing *COL7A1* cDNA without exon 70, and introduced the gene to keratinocytes from HS-RDEB patient who harbored heterozygous *COL7A1* 5818delC and 1474del8 mutations, and showed no expression of type VII collagen in immunofluorescence level as mentioned below (Goto *et al.*, 2006). The Western blot of the supernatant showed that HS-RDEB keratinocytes began to express type VII collagen after gene introduction (Figure 3a). The amounts of secreted collagen were almost identical in culture media between the normal *COL7A1* and *COL7A1*Δ70 samples. Subsequently, the cultured keratinocytes supernatant and the keratinocytes themselves were used for *in vitro* and *in vivo* studies. Cell migration assay using normal keratinocytes showed that the supernatants both with *COL7A1* and *COL7A1*Δ70 samples had a similar effect on the migration of normal keratinocytes (Figure 3b). The cell adhesion assay also demonstrated that *COL7A1*Δ70 supernatant had almost the same adhesive properties for the cells as normal *COL7A1* (Figure 3c). Furthermore, we constructed artificial skin grafts using untreated HS-RDEB fibroblasts and HS-RDEB keratinocytes transduced with *COL7A1* and *COL7A1*Δ70, and then applied them to a nude rat model. Ultrastructural analysis of the grafts showed formation of anchoring fibrils in both samples with *COL7A1* and *COL7A1*Δ70 samples (Figure 4). These results demonstrated that type VII collagen that lacks 16 amino acids of exon 70 might have similar properties to normal type VII collagen, suggesting that exon 70 skipping by AON is promising.

Elucidation of AON specific for 5818delC mutation

We designed mutation-specific AON hm70AON by deleting cytosine at 5818 (Figure 5a). Then we introduced hm70AON to normal human keratinocytes and HS-RDEB keratinocytes and performed the following RT-PCR analysis. The sample from HS-RDEB keratinocytes showed two PCR bands with or without exon 70, whereas a strong upper single band was observed in of the sample from normal human keratinocytes (Figure 5b). This indicated that the hm70AON induced skipping of exon 70 predominantly in abnormal allele with the 5818delC mutation. The sample from HS-RDEB keratinocytes without the AON treatment as control also showed the single band. TA cloning of the PCR samples showed that the exon skipping rates of HS-RDEB and normal keratinocyte samples were 18.5 and 1.3%, respectively; therefore, hm70AON induced skipping of exon 70 predominantly in abnormal allele with 5818delC. This HS-RDEB patient harbored heterozygous *COL7A1* 5818delC and 1474del8 mutations, and RT-PCR analysis using the keratinocyte cDNA showed no naturally occurring skipping of exon 70 containing the frameshift mutation (Figure 5b). Immunofluorescence analysis demonstrated using type VII collagen no expression of type VII collagen (Figure 5c) and ultrastructural study

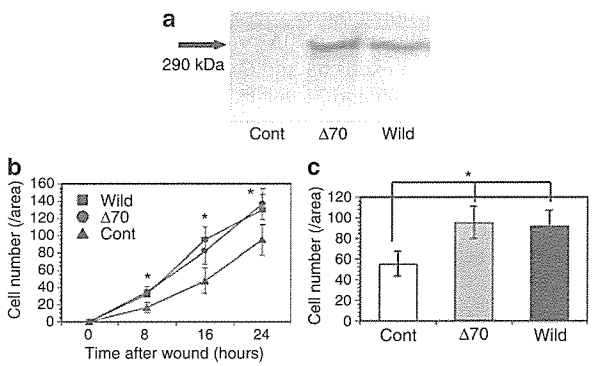

Figure 3. Assays for the type VII collagen without exon 70. We prepared retrovirus vectors with normal *COL7A1* cDNA (Wild) or *COL7A1* cDNA without exon 70 (Δ70), and introduced the gene into DEB keratinocytes, which showed no expression of any type VII collagen. (**a**) The Western blot of the supernatant showed that the amount of secreted type VII collagen in the culture media was almost similar to that of the normal *COL7A1* and *COL7A1*Δ70 samples. Cont: no transfection. (**b**) Cell migration assay showed that the supernatants from both *COL7A1* and *COL7A1*Δ70 samples had a similar effect on normal human keratinocyte migration. (**c**) The cell adhesion assay also demonstrated that *COL7A1*Δ70 supernatant had almost the same adhesive ability for normal keratinocytes as that of *COL7A1* (Figure 3). Each value represents mean ± SD of six samples. **P*<0.01: significant difference between cont *versus* wild or cont *versus* Δ70 samples.

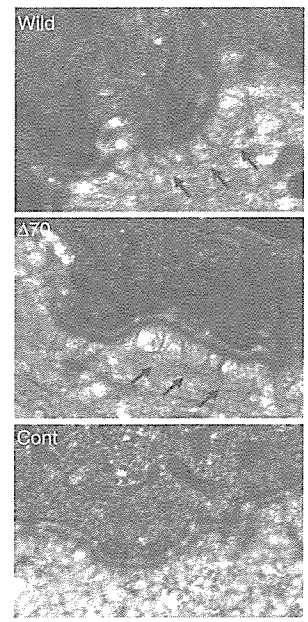

Figure 4. Formation of anchoring fibrils containing COL7A1Δ70. We constructed artificial skin grafts using DEB fibroblasts and keratinocytes transduced with wild-type *COL7A1* or *COL7A1*Δ70, and then grafted them onto a nude rat model. Ultrastructural analysis of the grafts showed that formation of anchoring fibrils could be identified in both samples with *COL7A1*- and *COL7A1*Δ70-transfected cells. Although no obvious anchoring fibrils were observed in control grafts with untransfected DEB keratinocytes alone (Cont), there were wisp-like structures below the lamina densa.

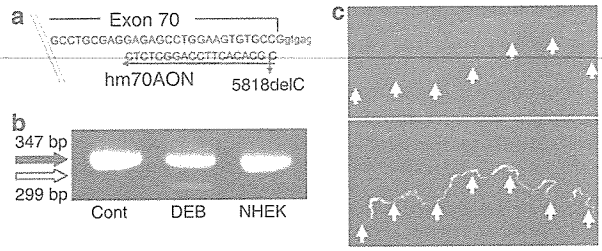

Figure 5. Elucidation of AONs specific for 5818delC mutation. We introduced mutation-specific AON hm70AON into normal human keratinocytes and DEB keratinocytes and performed the following RT-PCR analysis. (**a**) Sequences of mutation-specific AON hm70AON are shown. (**b**) The sample from DEB keratinocytes showed two PCR bands with exon 70 (347 bp) or without exon 70 (299 bp), whereas there was little or no lower band (299 bp) observed in the normal human keratinocytes sample (NHEK). Cont: the sample from DEB keratinocytes without the AON treatment. This HS-RDEB patient harbored heterozygous *COL7A1* 5818delC and 1474del8 mutations and RT-PCR analysis showed no naturally occurring skipping of exon 70 containing the frameshift mutation. (**c**) Immunofluorescence analysis of the patient using type VII collagen antibody demonstrated no expression of type VII collagen (the upper panel). The lower panel shows the expression from normal control. Arrows indicate epidermal-dermal junction.

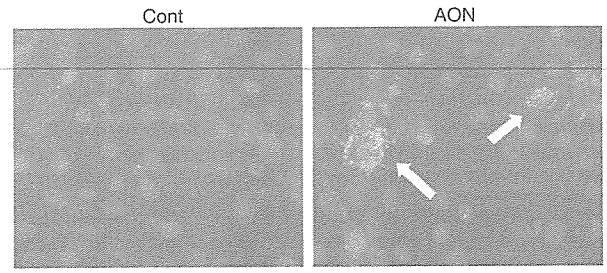

Figure 6. Rescue of type VII collagen expression in DEB keratinocytes *in vitro*. We transfected the hm70AON (AON) into cultured HS-RDEB keratinocytes and stained with an antibody against type VII collagen. Cont: no treatment of AON. Some cells were shown to express type VII collagen after the treatment (arrows).

revealed markedly reduced anchoring fibrils in the basement membrane zone (data not shown).

Rescue of type VII collagen expression in DEB keratinocytes *in vitro*

To examine *COL7A1* expression in the HS-RDEB keratinocytes treated with hm70AON, we transfected hm70AON into cultured HS-RDEB keratinocytes and stained with an antibody against type VII collagen (LH7.2). Some cells were shown to express type VII collagen (Figure 6). The rate of cell expression per total number of cells was 6.2%. We transfected h70AON1 and h70AON2, but no cells showed collagen VII immunoreactivity (data not shown).

Injection of hm70AON to the graft from DEB keratinocytes and fibroblasts

To determine the therapeutic feasibility of AON therapy in clinical practice, we constructed an artificial skin graft using HS-RDEB keratinocytes and fibroblasts, transplanted the graft to a nude rat, and then injected 30 μg of hm70AON to several portions of the graft. Saline was injected as a control. RT-PCR with the 66–72 primer set amplified only 347 bp band containing exon 70 and a weak signal for the 299 bp band without exon 70 from the treated sample (Figure 7a). The 70Δ primer set detected 305 bp band only in AON samples, indicating exon skipping of 70 (Figure 7b). Control samples did not express either 299 bp band by the 66–72 primer set, or 305 bp band using the 70Δ prime set. Furthermore, we performed immunohistochemical analysis of the treated graft with a type VII collagen antibody and could detect definite but intermittent linear dermal-epidermal junction immunoreactivity in the majority of treated samples, whereas no immunoreactivity was observed in control samples (Figure 7c and d).

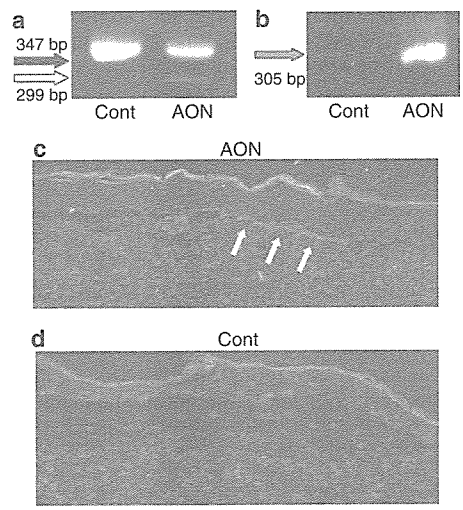

Figure 7. Injection of hm70AON into the graft from DEB keratinocytes and fibroblasts. We constructed an artificial skin graft using HS-RDEB keratinocytes and fibroblasts, transplanted the graft onto a nude rat, and then injected hm70AON into the graft. Saline was injected in a control. (**a**) RT-PCR with the 66–72 primer set amplified a 347 bp band containing exon 70 and a weak signal with the 299 bp band without exon 70 from the treated sample. (**b**) The 70Δ primer set detected only the 305 bp band in AON-treated samples. (**c**) Immunohistochemical analysis of the treated graft with type VII collagen antibody detected discontinuous, linear immunoreactivity along the dermal-epidermal junction (arrows). (**d**) Saline was injected in a control graft. Original magnification (**c**, **d**) ×200.

DISCUSSION

Type VII collagen, a non-fibrillar collagen, is a major component of anchoring fibril loop structures beneath the epidermal basement membrane (Uitto *et al.*, 1992; Burgeson, 1993). Cloning of collagen VII cDNA demonstrated a primary sequence of 2,944 amino acids and the basic organization of the functional domains (Christiano *et al.*, 1994a). Subsequent genomic cloning has highlighted the structural organization of the collagen VII gene (*COL7A1*) (Christiano *et al.*, 1994b).

This study has examined the feasibility of targeted exon skipping using AON. As the intron/exon organization of *COL7A1* contained 118 multiple short exons, deletion of one shorter exon may not significantly interfere with type VII collagen function. In fact, a mutation study revealed that several *COL7A1* splice-site mutations causing skipping of one exon resulted in a milder phenotype than the expected HS-RDEB that harbors nonsense mutations causing a lack of *COL7A1* expression (Terracina *et al.*, 1998). Furthermore, DEB mutations were frequently found in exons encoding collagenous domains and the nucleotide number of these exons is definite multiples of 3. This indicated that abolishment of exons restored an open leading flame of *COL7A1*. These characteristic features of the gene structure encouraged the start of research into the possibility of AON skipping therapy.

COL7A1 mutation database demonstrates presence of recurrent *COL7A1* mutation, and AONs, which are suitable for recurrent mutation, of course, are applicable for more patients than AONs for rare mutation. Thus, this study targeted exon 70 AON therapy, as the recurrent premature termination codon mutation 5818delC in exon 70 was found in more than 20% of recessive DEB sufferers (Tamai *et al.*, 1999; Sawamura *et al.*, 2005). We first synthesized two potential AONs, h70AON1 and h70AON2, for exon 70 and the results indicated that h70AON2 was able to induce skipping of exon 70 *in vitro* and *in vivo*. To understand the effect of exon 70 deletion on the essential functions of type VII collagen, we constructed *COL7A1* cDNA without exon 70 (*COL7A1*Δ70) and introduced this defective gene to HS-RDEB *in vitro* and *in vivo*. The results of attachment and migration analyses showed that the deleted collagen had an apparently similar function to the normal collagen. Next, we examined the ability of the defective collagen to form anchoring fibrils. To eliminate internal expression of type VII collagen, we used keratinocytes and fibroblasts from HS-RDEB who exhibited no *COL7A1* expression and failed to form any anchoring fibril-like structures in patient skin. Ultrastructural examination of the skin graft treated with *COL7A1*Δ70 demonstrated anchoring fibril formations in the sublamina densa. These results indicate that type VII collagen, lacking the 16 amino-acid sequences from exon 70, exhibits a remarkably near-normal assay similar to the normal type VII collagen.

As the sequence of h70AON2 was located at the 5818delC mutation site, we synthesized a mutation-specific AON hm70AON to match the sequence with deletion of 5818 cytosine. After transfection of hm70AON into HS-RDEB harboring the 5818delC defect, RT-PCR demonstrated effective exon 70 skipping. However, as predicted, when this AON was introduced to normal human keratinocytes, we found little skipping against exon 70 in the wild *COL7A1* allele. Some recessive DEB patients harbor heterozygous mutations 5818deC and missense mutations, which would not interfere with the function of this type VII collagen. In this case, hm70AON benefited by not altering the expression of *COL7A1* on the other allele. Further immunofluorescence studies using HS-RDEB cell culture systems showed that transfection of hm70AON could rescue type VII collagen expression in patient's keratinocytes. Approximately, 6% cells began to synthesize type VII collagen.

Finally, we constructed artificial HS-RDEB skin from the patient's keratinocytes and fibroblasts, and introduced hm70AON to the graft. RT-PCR analysis using the 66–72 primer set and the 70*Δ* primer set detected the presence of exon 70 skipping in the treated graft. Furthermore, immunofluorescence using type VII antibody demonstrated the positive expression of type VII collagen along restricted parts of the dermal–epidermal junction. Although we obtained the samples from several specimens and carried out electron microscopic analysis, we could not observe obvious anchoring fibrils ultrastructurally. We might examine no section corresponding to the restricted immunoreactive parts.

We recently suggested that fibroblasts might be a better gene therapy target of DEB treatment than keratinocytes (Goto *et al.*, 2006). The majority of collagen VII *in vivo* are thought to originate from keratinocytes because the level of *COL7A1* expression in the epidermis was much higher than that in the dermis. However, when *COL7A1* expressions of keratinocytes and fibroblast were almost equal after retroviral transfer of *COL7A1*, the gene-transferred fibroblasts supplied a higher amount of collagen VII to the new dermal–epidermal junction than the gene-transferred keratinocytes (Goto *et al.*, 2006). The AON therapy cannot generate an additional *COL7A1* expression, and it just modifies the existing expression. So, we think that AON transferred into keratinocytes gives predominant therapeutic effect in this study.

Finally, disadvantages of this AON approach for DEB are proposed. First, the effect disappeared immediately because AON is easily degraded in the cells. This study showed that the effect of AON was totally extinct 72 hours after the transfer of AON *in vitro*. Second, the method cannot induce the perfect full-length collagen VII. There is the possibility that in-frame exon skipping may lead to a dominant-negative interference. In fact, a 16-bp internal deletion in the *COL7A1* gene leading to in-frame exon skipping caused dominant phonotype of DEB (Cserhalmi-Friedman *et al.*, 1998). Third, transfer efficacy of AON to the skin is relatively low. Kinetic analysis of oligonucleotide topically applied to mouse skin showed early follicular localization, diffusion of the oligonucleotide from the mid-follicle, and subsequent dermal accumulation (Dokka *et al.*, 2005). Our study transfer efficacy was low in our skin graft experiment, but application of AON to actual skin may show a higher transfer efficacy, perhaps owing to the increased presence of skin appendages. In conclusion, we believe that improvement of these points enables this strategy to be applicable to clinical practice.

MATERIALS AND METHODS

AON

We selected exon 70 for AON therapy as the recurrent premature termination codon mutation 5818delC was present in exon 70 in DEB patients (Tamai *et al.*, 1999; Sawamura *et al.*, 2005). We designed a potential AON for exon skipping using the RNA mfold version 3.1 server (Zuker, 2003), and synthesized a full-length phosphorothioate backbone and HPLC-purified 2′-*O*-methyl-modified ribose

molecules. The sequences of the synthesized AONs were as follows: h70AON1, 5′-CCACGCUCUCCAGGGAG-3′ and h70AON2, 5′-CUUCCAGGCUCUCCUCGC-3′ for human type VII collagen: hm70AON, 5′-CGCACACUUCCAGGC-3′ for 5818delC mutation (Figures 1a and 5b).

Cell culture and AON transfection

The human keratinocyte HaCaT cell line was maintained in DMEM with 10% fetal bovine serum. Primary keratinocytes were isolated and grown in the presence of mitomycin C-treated 3T3 feeder layer (Rheinwald and Green, 1975). Briefly, keratinocytes, which were obtained from HS-RDEB patient skin biopsies and healthy controls, were cultured on feeder layers of mitomycin C-treated mouse 3T3 fibroblasts in DMEM: Ham's F-12 (3:1) supplemented with 10% fetal bovine serum, 5 μg/ml insulin, 10 ng/ml EGFR, 0.4 μg/ml hydrocortisone, and 8 ng/ml cholera toxin. Human fibroblasts were also obtained from a skin biopsy from an HS-RDEB patient and healthy controls, and were cultured in DMEM with 10% fetal bovine serum. This HS-RDEB patient harbored heterozygous *COL7A1* 5818delC and 1474del8 mutations, and showed no expression of type VII collagen (Goto *et al.*, 2006).

After changing of the medium to serum-free Opti-MEM (Gibco Invitrogen, Grand Island, NY), we transfected the AONs into the cells using Lipofectamine 2000 (Gibco Invitrogen) according to the manufacturer's protocols. In all experiments, the cells were exposed to transfection reagent for 16 hours and the media were replaced with fresh growth medium.

Graft experiments

We transplanted artificial and normal skin onto a nude rat. Briefly, 10^6 HS-RDEB fibroblasts were seeded into a collagen sponge scaffold and maintained in DMEM with 10% fetal bovine serum. Confluent cultures containing 10^6 HS-RDEB keratinocytes were treated with dispase (1 nU/ml; Godo Shusei, Tokyo, Japan), and the floating epidermal sheet placed on the collagen sponge. In nude rats (F344/N Jcl-rnu; CLEA Japan, Tokyo, Japan), the sites for transplantation were prepared by excising a 2 cm^2 area of dorsal skin. The collagen sponge containing the fibroblasts was placed into the skin wound and then the epidermal sheet overlaid on the collagen sponge. In other experiments, normal skin samples were obtained from the abdomens of patients undergoing reconstructive plastic surgery at the Hokkaido University Hospital. Each skin sample was placed directly on the 2 cm^2 wound on the nude rat. Afterwards, an occlusive dressing was quickly placed over the graft to hold it in position and to prevent it from drying. After 7 days, the dressing was removed, and then 30 μg AON was diluted in normal saline to a final volume of 150 μl and injected into several portions of the grafts. After 16 hours, the skin biopsies were taken from the injected site and were subjected to RT-PCR analysis as the *in vitro* time-course study indicated the highest expression of the exon-skipping band at 16 hours after AON transfer.

Informed consents were obtained from all individual subjects in this study. The protocols were approved by the Ethical Committee at Hokkaido University Graduate School of Medicine. This study was conducted according to the Declaration of Helsinki Principles.

RNA isolation and RT-PCR analysis

Skin samples were taken from the rodent model and were first homogenized using a Polytron homogenizer. Total RNA was extracted from skin samples and cultured cells using an RNeasy RNA extraction kit (Qiagen, Hilden, Germany). First strand cDNA was synthesized with reverse transcriptase (Life Sciences, St Petersburg, FL) using an oligo-dT primer. To determine the splice-specific expression of exon 70, we designed the forward PCR primer on the border of exons 65 and 66, and the reversel primer on exon 72. The amplification conditions were carried out using the 66–72 primer set, forward 5′-GAAGGGAGAGAAAGGAGATT-3′ and reversel 5′-GGAAGCTACCAGAGCTCTCA-3′, for 35 cycles of reaction at 94°C for 1 minute, 58°C for 1 minute, and 72°C for 1 minute. In addition, to verify the skipping of exon 70, we set the forward primer on the border of exons 63 and 64, and reversel primer on the border of exons 69 and 71. The amplification conditions were carried out with the 70Δ primer set, forward 5′-TGGATTACCGGGAAAGCCAG-3′ and reversel 5′-GATCCACATTCTGCTCCCCT-3′, for 35 cycles of reaction at 94°C for 1 minute, 58°C for 1 minute, and 72°C for 1 minute. The PCR products were fractionated on 2% agarose gels and directly sequenced by di-deoxy dye-terminator method using an automated sequencer (ABI Prism Genetic Analyzer 3100, PE Biosystems, Foster city, CA). When several bands were found, we subcloned the PCR sample into a TA cloning vector (Gibco Invitrogen). After transformation of the bacteria, we picked up 50 colonies and examined the inserts to semiquantify the amounts of the bands. The rate of the lower band to the upper band was expressed as the exon skipping rate. Each value represents the mean ± SD of four samples. Moreover, the PCR products were directly sequenced by di-deoxy dye-terminator method using an automated sequencer (ABI Prism Genetic Analyzer 3100, PE Biosystems, Foster city, CA).

Immunostaining and Western blot analysis. Cultured, transfected cells were fixed with 2% paraformaldehyde in phosphate-buffered saline, and were then incubated with the mAb LH7.2 against the NC1 domain of collagen type VII (Chemicon, Temecula, CA). The secondary antibody was FITC-conjugated goat anti-mouse IgG and preparations were examined under a fluorescence microscope. Subconfluent keratinocyte cultures were fed for 48 hours with serum-free medium supplemented with 50 μg/ml ascorbic acid. For SDS-PAGE analysis, the culture medium was treated with Amicon Ultra-100,000 Centrifugal Filter Devices (Millipore, Bedford, MA) for protein concentration and desalting. The samples were separated on a 5% polyacrylamide gel under reducing conditions. Immunoblotting analysis was performed using the LH7.2 mAb followed by the secondary antibody goat anti-mouse IgG conjugated to peroxidase. The resultant complexes were processed for Phototope horse radish peroxidase Western Blot Detection System (Cell Signaling, Beverly, MA) according to the manufacturer's protocol.

Assays for the type VII collagen without exon 70

Introduction of h70AON2 into keratinocytes induced skipping of exon 70 (see the Results section). We prepared cDNA from the introduced keratinocytes and amplified cDNA without exon 70 (*COL7A1*Δ70). A retroviral vector pDON(Δ) was created by removing the Simian virus-40 promoter and *Neo* gene from pDON-AI (Takara, Kyoto, Japan). The genes *COL7A1* and *COL7A1*Δ70 were inserted into pDON(Δ) and these retrovirus plasmids were introduced into the amphotropic amphopack-293 packaging cells (Clontech, Palo Alto, CA) using calcium phosphate co-precipitation.

The viral particles were recovered from the cell culture medium 48 hours later and applied to cultured DEB keratinocytes that failed to express *COL7A1*. The supernatant of the cultured keratinocytes and the keratinocytes themselves were used for *in vitro* and *in vivo* studies.

The methods for the cell migration assay and cell adhesion assay were performed as described previously (Tsuda *et al.*, 2002). Briefly, culture dishes were treated with conditioned supernatants from cultured HS-RDEB keratinocytes transduced with *COL7A1* and *COL7A1*Δ70 for 24 hours. Control dishes were treated with culture medium. After the plating of normal keratinocytes for 48 hours on the treated dishes, the cells were scraped off using a 200 μl yellow pipette tip. Subsequently, at 8, 16, and 24 hours, the number of cells that had moved from the base line into the scratched area was measured. In addition, normal keratinocytes were allowed to attach for 1.5 hours on the treated dishes and, after removal of unattached cells, washed and fixed with 70% ethanol for 10 minutes. Adherent cells were then stained with crystal violet and the number of the cells was measured.

The collagen sponge containing HS-RDEB fibroblasts was placed on skin wound of nude rat and the confluent cultures of 10^6 HS-RDEB keratinocytes transduced with *COL7A1* and *COL7A1*Δ70 were overlaid on the collagen sponge, as mentioned above. After 8 weeks, the skin biopsies were taken from the graft and subject to routine ultrastructural analysis.

CONFLICT OF INTEREST

The authors state no conflict of interest.

ACKNOWLEDGMENTS

This work was supported in part by Grants-in-Aid from the Ministry of Education, Science, Sports, and Culture of Japan to Sawamura D. (15390337, 17659331) and Shimizu H. (15390336, 17209038), and by grants from the Ministry of Health of Japan to Shimizu H. (H16-Intractable Disease-05).

REFERENCES

Burgeson RE (1993) Type VII collagen, anchoring fibrils, and epidermolysis bullosa. *J Invest Dermatol* 101:252–5

Chen M, Kasahara N, Keene DR, Chan L, Hoeffler WK, Finlay D *et al.* (2002) Restoration of type VII collagen expression and function in dystrophic epidermolysis bullosa. *Nat Genet* 32:670–5

Christiano AM, Greenspan DS, Lee S, Uitto J (1994a) Cloning of human type VII collagen, complete primary sequence of the alpha 1(VII) chain and identification of intragenic polymorphisms. *J Biol Chem* 269: 20256–62

Christiano AM, Hoffman GG, Chung-Honet LC, Lee S, Cheng W, Uitto J *et al.* (1994b) Structural organization of the human type VII collagen gene (COL7A1) composed of more exons than any previously characterized gene. *Genomics* 21:169–79

Cserhalmi-Friedman PB, McGrath JA, Mellerio JE, Romero R, Salas-Alanis, Paller AS *et al.* (1998) Restoration of open reading frame resulting from skipping of an exon with an internal deletion in the COL7A1 gene. *Lab Invest* 78:1483–92

Dokka S, Cooper SR, Kelly S, Hardee GE, Karras JG (2005) Dermal delivery of topically applied oligonucleotides via follicular transport in mouse skin. *J Invest Dermatol* 124:971–5

England SB, Nicholson LV, Johnson MA, Forrest SM, Love DR, Zubrycka-Gaarn EE *et al.* (1990) Very mild muscular dystrophy associated with the deletion of 46% of dystrophin. *Nature* 343:180–2

Galderisi U, Cascino A, Giordano A (1999) Antisense oligonucleotides as therapeutic agents. *J Cell Physiol* 181:251–7

Goto M, Sawamura D, Ito K, Abe M, Nishie W, Sakai K *et al.* (2006) Fibroblasts show more potential target cells than keratinocytes for COL7A1 gene therapy of dystrophic epidermolysis bullosa. *J Invest Dermatol* 126:766–72

Fine JD, Eady RA, Bauer EA, Briggaman RA, Bruckner-Tuderman L, Christiano A *et al.* (2000) Revised classification system for inherited epidermolysis bullosa: report of the Second International Consensus Meeting on diagnosis and classification of epidermolysis bullosa. *J Am Acad Dermatol* 42:1051–66

Lu QL, Mann CJ, Lou F, Bou-Gharios G, Morris GE, Xue SA *et al.* (2003) Functional amounts of dystrophin produced by skipping the mutated exon in the mdx dystrophic mouse. *Nat Med* 9:1009–14

Mann CJ, Honeyman K, Cheng AJ, Ly T, Lloyd F, Fletcher S *et al.* (2001) Antisense-induced exon skipping and synthesis of dystrophin in the mdx mouse. *Proc Natl Acad Sci USA* 98:42–7

Mayeda A, Hayase Y, Inoue H, Ohtsuka E, Ohshima Y (1990) Surveying cis-acting sequences of pre-mRNA by adding antisense 2′-*O*-methyl oligoribonucleotides to a splicing reaction. *J Biochem* 108:399–405

McGrath JA, Ashton GH, Mellerio JE, Salas-Alanis JC, Swensson O, McMillan JR *et al.* (1999) Moderation of phenotypic severity in dystrophic and junctional forms of epidermolysis bullosa through in-frame skipping of exons containing non-sense or frameshift mutations. *J Invest Dermatol* 113:314–21

Monaco AP, Bertelson CJ, Liechti-Gallati S, Moser H, Kunkel LM (1988) An explanation for the phenotypic differences between patients bearing partial deletions of the DMD locus. *Genomics* 2:90–5

Ortiz-Urda S, Thyagarajan B, Keene DR, Lin Q, Fang M, Calos MP *et al.* (2002) Stable nonviral genetic correction of inherited human skin disease. *Nat Med* 8:1166–70

Rheinwald JG, Green H (1975) Serial cultivation of strains of human epidermal keratinocytes: the formation of keratinizing colonies from single cells. *Cell* 6:331–43

Sawamura D, Goto M, Yasukawa K, Sato-Matsumura N, Nakamura H, Ito K *et al.* (2005) Genetic studies of 20 Japanese families of dystrophic epidermolysis bullosa. *J Hum Genet* 50:543–6

Tamai K, Murai T, Mayama M, Kon A, Nomura K, Sawamura D *et al.* (1999) Recurrent COL7A1 mutations in Japanese patients with dystrophic epidermolysis bullosa: positional effects of premature termination codon mutations on clinical severity. *J Invest Dermatol* 112:991–3

Terracina M, Posteraro P, Schubert M, Sonego G, Atzori F, Zambruno G *et al.* (1998) Compound heterozygosity for a recessive glycine substitution and a splice site mutation in the COL7A1 gene causes an unusually mild form of localized recessive dystrophic epidermolysis bullosa. *J Invest Dermatol* 111:744–50

Tsuda M, Tanaka S, Sawa H, Hanafusa H, Nagashima K (2002) Signaling adaptor protein v-Crk activates Rho and regulates cell motility in 3Y1 rat fibroblast cell line. *Cell Growth Differ* 13:131–9

Uitto J, Chung-Honet LC, Christiano AM (1992) Molecular biology and pathology of type VII collagen. *Exp Dermatol* 1:2–11

Uitto J, Hovnanian A, Christiano AM (1995) Premature termination codon mutations in the type VII collagen gene (COL7A1) underlie severe recessive dystrophic epidermolysis bullosa. *Proc Assoc Am Phys* 107:245–52

Wessagowit V, Kim SC, Woong Oh S, McGrath JA (2005) Genotype-phenotype correlation in recessive dystrophic epidermolysis bullosa: when missense doesn't make sense. *J Invest Dermatol* 124:863–6

Zuker M (2003) Mfold web server for nucleic acid folding and hybridization prediction. *Nucleic Acids Res* 31:3406–15

ORIGINAL ARTICLE

Compound Heterozygous Mutations Including a *De Novo* Missense Mutation in *ABCA12* Led to a Case of Harlequin Ichthyosis with Moderate Clinical Severity

Masashi Akiyama[1], Kaori Sakai[1], Yoriko Sugiyama-Nakagiri[1], Yasuko Yamanaka[1], James R. McMillan[2], Daisuke Sawamura[1], Hironori Niizeki[3], Sachiko Miyagawa[3] and Hiroshi Shimizu[1]

Harlequin ichthyosis (HI) is one of the most devastating genodermatoses. Recently, *ABCA12* mutations were identified as the cause of HI. A newborn Japanese male demonstrated the typical features of HI. The patient was treated with oral etretinate and his general condition has been good (now aged 1.5 years). This patient with moderate clinical severity was compound heterozygous for a novel *de novo* missense mutation 1160G>A (S387N) in exon 10 and a maternal deletion mutation 4158_4160delTAC (T1387del) in exon 28 of *ABCA12*. T1387del was a deletion of a highly conserved threonine residue within the first adenosine 5′ triphosphate-binding domain and is thought to seriously affect the function of the ABCA12 protein. Conversely, the residue 387 is located outside the known active sites of ABCA12 and S387N is predicted not to lead to a serious functional deficiency in ABCA12. Electron microscopy revealed abnormal lamellar granules in the granular layer cells and a moderate number of lipid vacuoles in the cornified cells. Disturbed glucosylceramide transport was confirmed in the cultured keratinocytes from the patient. No *de novo* mutation in *ABCA12* has yet been reported either in HI or lamellar ichthyosis. The present case suggested that a *de novo ABCA12* mutation might underlie HI.

Journal of Investigative Dermatology (2006) **126,** 1518–1523. doi:10.1038/sj.jid.5700295; published online 4 May 2006

INTRODUCTION

Harlequin ichthyosis (HI) (MIM no. 242500) is a severe and often fatal congenital ichthyosis with an autosomal recessive inheritance pattern (Williams and Elias, 1987; Akiyama, 1999; Judge *et al.*, 2004).

In 2005, *ABCA12* mutations were identified in HI families (Akiyama *et al.*, 2005; Kelsell *et al.*, 2005). The pathomechanisms of HI became known when functional defects in the lipid transporter ABCA12 were shown to cause abnormal lipid transport via lamellar granules (LGs) in the keratinocytes, resulting in malformation of the patient's intercellular lipid layers of the stratum corneum (Akiyama *et al.*, 2005). However, genotype/phenotype correlations in HI cases with *ABCA12* mutations have yet to be fully elucidated (Akiyama, in press a).

In the study of this case, we have found a compound heterozygous *ABCA12* combination of mutations, a novel *de novo* missense mutation, S387N, in exon 10 and a maternal deletion mutation T1387del in exon 28 in a newborn HI baby. In the majority of HI patients, deletion or truncation mutations seriously affecting ABCA12 function were found. However, in the present case, one mutation was a missense mutation located in the cytoplasmic region of ABCA12 polypeptide, not in the transmembrane domain or the adenosine 5′ triphosphate (ATP)-binding cassettes. The nature and site of mutations might be the key to the relatively moderate phenotype of this HI patient.

In addition, the novel mutation S387N was the first reported *de novo* mutation in *ABCA12*. Our case suggested the possibility that *de novo* mutations can cause the occurrence of HI in non-consanguineous families.

RESULTS

Clinico-pathological features of the patient

The patient was a newborn Japanese male. He was born at 33 weeks and 3 days pregnancy by premature, vaginal delivery (body weight 1,876 × *g*). He was the first child of non-consanguineous healthy parents. There was no family history of congenital ichthyosis. At birth, the patient had presented with severe hyperkeratosis over his entire body, severe ectropion, eclabium, and malformed pinnae (Figure 1). The patient's clinical features at birth were characteristic of typical HI. He was admitted into a neonatal intensive care unit and had oral etretinate treatment (1 mg/kg/day). At this time, light microscopy of the lesional skin sample from the patient's trunk showed marked hyperkeratosis with only a

[1]*Department of Dermatology, Hokkaido University Graduate School of Medicine, Sapporo, Japan;* [2]*Creative Research Initiative Sousei, Hokkaido University, Sapporo, Japan and* [3]*Department of Dermatology, Nara Medical University School of Medicine, Kashihara, Japan*

Correspondence: Dr Masashi Akiyama, Department of Dermatology, Hokkaido University Graduate School of Medicine, North 15 West 7, Kita-ku, Sapporo 060-8638, Japan. E-mail: akiyama@med.hokudai.ac.jp

Abbreviations: ATP, adenosine 5′ triphosphate; HI, harlequin ichthyosis; LG, lamellar granule

Received 28 November 2005; revised 13 February 2006; accepted 16 February 2006; published online 4 May 2006

Figure 1. The patient showed a typical clinical phenotype of HI in the neonatal period. The entire body surface was covered with thick plate-like scales and fissures.

small number of parakeratotic cells. At the age of 1 year, the patient showed dark brownish, thick scales over the entire body surface including the face, palms, and the soles.

ABCA12 mutation analysis

Mutation analysis of the 53 exons including the intron–exon boundaries of the entire *ABCA12* gene revealed a 1160G>A transition in exon 10 and one previously reported deletion mutation 4158_4160delTAC in exon 28 in each allele in a compound heterozygous fashion in the patient (sequence according to Lefèvre *et al.* (2003)) (GenBank accession NM 173076) (Figure 2). The mutation 1160G>A transition was a novel missense mutation that changed a serine residue of codon 387 to an asparagine residue (S387N). This missense mutation S387N was not found in either in the parent's (father or mother), although the patient's mother was heterozygous for the deletion mutation 4158_4160delTAC (Figure 2). Thus, the missense mutation S387N was thought to be a *de novo* mutation and the deletion mutation was a maternal mutation. Paternity testing by microsatellite marker analysis proved the father was the patient's true genetic father (data not shown). These mutations were not found in 200 normal, unrelated Japanese alleles (100 normal unrelated Japanese individuals) by sequence analysis, and were unlikely to be a polymorphism (data not shown). The deletion mutation 4158_4160delTAC led to an in-frame deletion of a highly conserved threonine residue at codon 1387 (T1387del) within the first ATP-binding

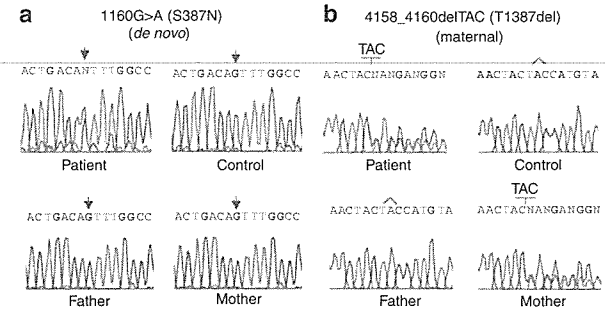

Figure 2. Compound heterozygous mutations of ABCA12 in the patient. (**a**) Direct sequencing revealed a heterozygous 1160G>A transition (a missense mutation S387N) in exon 10 of *ABCA12* of the patient, but not in his parents or normal control samples. (**b**) A heterozygous deletion mutation 4158_4160delTAC (T1387del) was found in exon 28 of *ABCA12* of the patient and his mother, but not in his father or in normal controls.

domain of ABCA12. Thus, the deletion mutation is thought to seriously affect either the function or specific critical structures of the ABCA12 protein (Akiyama *et al.*, 2005).

Ultrastructure of the patient's skin

Electron microscopy revealed that, in the keratinocyte cytoplasm of the granular layer, no normal LGs were apparent. Lipid droplets, vacuoles, and multivesiculated bodies were seen in keratinocytes in the keratinized and granular cell layers (Figure 3a and b). The number of abnormal lipid droplets in the keratinized stratum corneum cells was smaller than that in skin samples from HI patients harboring the homozygous splice acceptor site mutation IVS23-2A>G of *ABCA12* (Akiyama *et al.*, 2005) (Figure 3c), although the number of lipid vacuoles was larger than those in lamellar ichthyosis patients with *ABCA12* mutations (data not shown). Cornified cell envelope formation was normal in the granular and cornified layer cells (Figure 3h).

Distribution of ABCA12 and glucosylceramide in patient's skin

Immunofluorescence studies revealed that ABCA12 was positive in the upper epidermal layers, mainly in the granular layers, of normal human skin (Figure 4c). In the epidermis of the present patient, reduced ABCA12 immunostaining was seen in the upper epidermis (Figure 4a), compared with seriously reduced immunolabeling in epidermal keratinocytes from the HI patient harboring a homozygous splice acceptor site mutation IVS23-2A>G (Figure 4b) (Akiyama *et al.*, 2005). These findings confirmed that the present patient expresses a significant amount of mutated ABCA12 protein in his epidermis.

Immunofluorescent staining showed that glucosylceramide, a major lipid component of LGs (Vielhaber *et al.*, 2001; Ishida-Yamamoto *et al.*, 2004) and an essential component of the epidermal permeability barrier (Holleran *et al.*, 1993), was sparsely distributed in the patient's upper epidermis (Figure 4a), compared with a restricted, intense distribution in the granular layers of normal skin (Figure 4c). The condensed glucosylceramide staining was not seen in the patient's granular layers (Figure 4a).

Abnormal glucosylceramide transport in patient's cultured keratinocytes

Culture of the patient's keratinocytes under high-Ca^{2+} conditions (2.0 mM) induced a large number of cells to express condensed glucosylceramide staining around the nuclei, and this glucosylceramide failed to become localized to the periphery of the keratinocyte cytoplasm (Figure 5a). Culture of normal human keratinocytes in high-Ca^{2+} conditions exhibited a more diffuse glucosylceramide staining throughout the cytoplasm (Figure 5b).

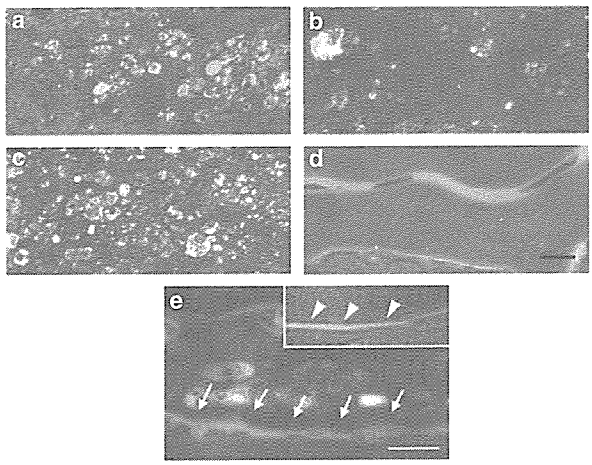

Figure 3. Abnormal LGs in the granular layer cells and accumulation of lipid droplets in the stratum corneum cells of the patient's epidermis. (**a**) Abnormal LGs in the granular layer cells of the patient. (**b**) Abnormal lipid droplets accumulated in the cornified cells in the patient's epidermis, although the numbers and amounts of lipid droplets was smaller than that seen in an HI patient harboring a homozygous splice acceptor site mutation IVS23-2A>G of *ABCA12* (**c**). (**d**) No lipid droplets were observed in control normal human stratum corneum cells. (**a, b**) the present patient; (**c**) control typical HI patient reported previously (Akiyama *et al.*, 2005); (**d**) normal control human skin. (**e**) Cornified cell envelope (arrows) with normal thickness was seen in the cornified layer cells in the present HI patient. Inset: the cornifed layer cell of the control lamellar ichthyosis patient with transglutaminase 1 gene mutations showed malformed, thin cornified cell envelope (arrowheads). Bars = 200 nm.

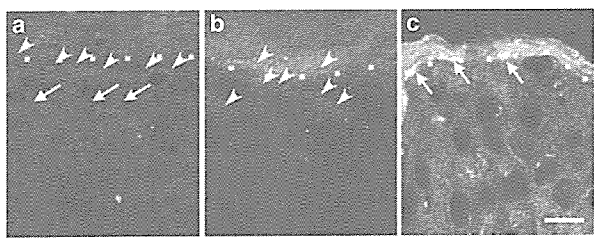

Figure 4. Abnormal ABCA12 immunostaining and disturbed distribution of glucosylceramide in the patient's epidermis. (**a**) In the patient's upper epidermis, weak ABCA12 immunostaining (red: arrows) was diffusely seen in the keratinocyte cytoplasm. Glucosylceramide labeling (green: arrowheads) was also diffusely observed in the keratinocytes of upper epidermis. (**b**) In the control HI patient carrying a homozygous splice acceptor site mutation IVS23-2A>G of *ABCA12*, ABCA12 immunolabeling (red) was very weak, although diffuse glucosylceramide immunolabeling (green: arrowheads) was seen in the keratinocyte cytoplasm of upper epidermis. (**c**) In normal control human epidermis, both ABCA12 (red) and glucosylceramide (green) labelings overlapped, resulting in a yellow color in the granular layer (arrows). Dotted line; granular layer–cornified layer interface. ABCA12, tetramethylrhodamine isothiocyanate (red); glucosylceramide, FITC (green); nuclear staining, TO-PRO (blue). Bar = 10 μm.

DISCUSSION

The ATP-binding cassette (ABC) transporter superfamily is one of the largest gene families, encoding a highly conserved group of proteins involved in energy-dependent active transport (Higgins, 1992; Allikmets *et al.*, 1996; Dean *et al.*, 2001; Borst and Elferink, 2002) and, recently, this superfamily has been highlighted in the dermatology fields (Uitto, 2005). The ABCA subfamily is suggested to work in lipid transport (Weng *et al.*, 1999; Hayden *et al.*, 2000; Orso *et al.*, 2000; Schmitz and Langmann, 2001; Peelman *et al.*, 2003) and has received considerable attention (Klein *et al.*, 1999) because mutations in these genes have been implicated in several human genetic diseases (Allikmets *et al.*, 1997a, b; Brooks-Wilson *et al.*, 1999; Rust *et al.*, 1999; Oram, 2002). Keratinocyte LGs are known lipid-transporting organelles and LG contents are secreted into the intercellular space, forming an intercellular lipid layer between the granular layer cells and keratinized cells in the stratum corneum. Our previous study (Akiyama *et al.*, 2005) has clearly demonstrated that ABCA12 functions in the transport of endogenous lipid to the keratinocyte cell periphery via LGs.

The abnormal LGs in the granular layer keratinocytes and a lack of extracellular lipid lamellae reflect the defective lipid transport via LGs and the malformation of intercellular stratum corneum lipid layer in HI (Akiyama, in press a). In 2005, *ABCA12* mutations that seriously affect its function were shown to cause a loss of the skin lipid barrier, leading to HI (Akiyama *et al.*, 2005). In addition to HI with defective lipid layers in the stratum corneum, ichthyosis syndromes are also thought to share similar pathomechanisms (Akiyama, in press b). For example, Dorfman–Chanarin syndrome (neutral lipid storage disease) showed malformation of LGs and

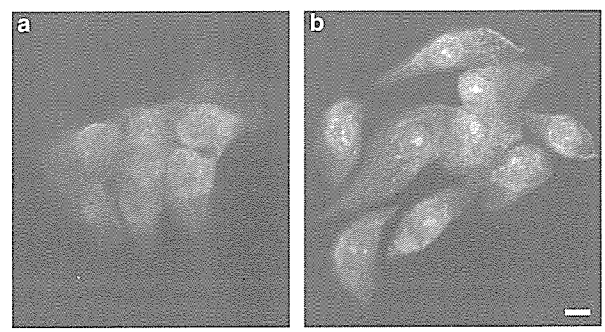

Figure 5. Altered glucosylceramide distribution in the patient's cultured keratinocytes. (**a**) In keratinocytes cultured from the patient, glucosylceramide labeling (green) was observed mainly in the perinuclear area of cytoplasm, suggesting disturbed glucosylceramide transport. (**b**) In normal cultured human keratinocytes, glucosylceramide (green) was seen diffusely in the cytoplasm to the cell periphery. Glucosylceramide, FITC (green); nuclear staining, propidium idodide (red). Bar = 10 μm.

defective lipid production in LGs caused by a deficiency in the CGI-58 protein that is thought to be involved in the pathogenesis of this form of ichthyosis (Akiyama *et al.*, 2003). In Sjögren–Larsson syndrome harboring fatty aldehyde dehydrogenase (FALDH) gene (*ALDH3A2*) mutations, defective LG formation was reported as one sign of a putative pathogenetic mechanism (Shibaki *et al.*, 2004). Recently, mutations in a new gene, *FLJ39501*, encoding a cytochrome *P*450, family 4, subfamily F, polypeptide 2 homolog of the leukotriene B4-ω-hydroxylase (CYP4F2) were reported to underlie lamellar ichthyosis cases linked to chromosome 19p12-q12 (Lefèvre *et al.*, 2006). These facts further support the idea that abnormal LG lipid contents and defective intercellular lipid are prevailing concepts of pathogenetic mechanisms in the ichthyoses.

In the present case based on the reported amino-acid sequence (Annilo *et al.*, 2002), the deletion mutation 4158_4160delTAC led to an in-frame deletion of a threonine residue at codon 1387 (T1387del) within the first ATP-binding domain of ABCA12 protein (Figure 6). This threonine residue is a highly conserved residue between diverse species and is thought to be important in the function of ABCA12 (Akiyama *et al.*, 2005). Indeed, a compound heterozygous patient with this deletion mutation and a separate *ABCA12* truncation mutation was previously reported as a typical HI newborn who died 15 days after birth (Akiyama *et al.*, 2005).

The novel *de novo* mutation S387N in the present patient is located outside all of the known ABCA12 active transporter sites, within the cytoplasmic domain at N-terminus of ABCA12 polypeptide (Figure 6). Both serine and asparagine are neutral amino acids with small side chains and this missense mutation would be expected to not significantly affect the conformation of ABCA12 molecule. Thus, one would predict the *de novo* missense mutation S387N not to lead to a serious ABCA12 functional loss. Considering the nature and site of the *ABCA12* mutations in this case, we suggest that a combination of the deletion mutation and the missense mutation leads to the current patient's HI phenotype with a moderate clinical severity.

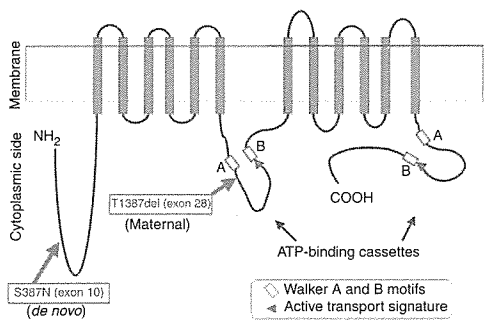

Figure 6. Schematic sequential arrangement of the domain structures of ABCA12 protein and the position of mutations in the present HI patient. Mutations in the present HI patient are marked by red arrows. Note that the *de novo* missense mutation S387N is located in the intracytoplasmic region between the N-terminus and the first transmembrane domain, not in any active sites, and the other, deletion mutation T1387del is within the first ATP-binding cassette, which is thought to be important for ABCA12 lipid transporter activity.

In type 2 lamellar ichthyosis, a relatively mild form of congenital ichthyosis, all five reported *ABCA12* mutations were missense mutations that resulted in only one amino-acid alteration (Lefèvre *et al.*, 2003). Conversely, in our previous study on HI families, no *ABCA12* missense mutations were identified and most of the defects led to severe truncation of ABCA12 peptide, affecting important nucleotide-binding fold domains and/or transmembrane domains (Akiyama *et al.*, 2005). The other, non-truncation mutations in HI were deletion mutations affecting highly conserved *ABCA12* sequences (Akiyama *et al.*, 2005). Thus, it was thought that only truncation or deletion mutations in conserved regions, which seriously affect the function of the ABCA12 transporter protein, can lead to the HI phenotype.

In an additional series of HI patients, most *ABCA12* mutations were homozygous truncation mutations (Kelsell *et al.*, 2005). Only one mutation in one HI patient was a missense mutation and the patient was heterozygous for a truncation mutation and the missense mutation.

Recently, the prognosis of newborns affected with HI has improved, owing to better targeted oral retinoid treatment. More than half of HI newborns including cases with a serious functional loss of ABCA12 survive beyond the perinatal period (Akiyama *et al.*, 2005; Akiyama, in press a). Thus, it is difficult to discuss genotype/phenotype correlations and quality of life prognosis for *ABCA12* mutations in HI.

Most families with HI or lamellar ichthyosis caused by *ABCA12* mutations were consanguineous and, in those families, causative *ABCA12* mutations were homozygous mutations inherited with an autosomal recessive trait. No *de novo* mutation has yet been reported in *ABCA12*, as far as we know (Lefèvre *et al.*, 2003; Akiyama *et al.*, 2005; Kelsell *et al.*, 2005). The present novel missense mutation S387N in our case was the first *de novo* mutation reported in *ABCA12*. The genetic information of whether the causative mutations are inherited or *de novo* is very important for genetic counseling in severe genetic disorders such as HI. Indeed, in the present family, the parents had requested a prenatal diagnosis of HI for their subsequent pregnancy. However, we have demonstrated that the missense mutation was a *de novo* mutation and that the patient's father was not a carrier of any *ABCA12* mutation. Thus, the family could be spared of the worry of an unnecessary HI prenatal diagnosis for the subsequent pregnancy almost, although we cannot completely exclude the possibility that the father has a mosaic mutation affecting his germ line. The present case suggested that, in non-consanguineous HI families, a *de novo ABCA12* mutation might be one source of mutations and underlines that the detection of causative *ABCA12* mutations is essential for the genetic counseling for HI.

MATERIALS AND METHODS

Mutation detection

Mutational analysis was performed in the affected baby and the parents. Briefly, genomic DNA isolated from peripheral blood was subjected to PCR amplification, followed by direct automated

sequencing using an ABI PRISM 3100 genetic analyzer (ABI Advanced Biotechnologies, Columbia, MD). Oligonucleotide primers and PCR conditions used for amplification of all exons 1–53 of *ABCA12* were originally derived from the report by Lefèvre *et al.* (2003) and were partially modified for the present study. The entire coding region including the exon/intron boundaries for both forward and reverse strands from the patient, family members, and 100 healthy Japanese controls were sequenced. No mutations were found in 200 normal alleles from the healthy Japanese population. Paternity testing was carried out using 16 microsatellite markers. The parents provided informed consent to the experiments. The experiments received institutional approval and the protocol adhered to The Declaration of Helsinki Principles.

Ultrastructural observations

Skin biopsy samples were fixed in 5% glutaraldehyde solution, post-fixed in 1% OsO_4, dehydrated, and embedded in Epon 812. The samples were sectioned at 1 μm thickness for light microscopy and thin sectioned for electron microscopy (70 nm thick). The thin sections were stained with uranyl acetate and lead citrate and examined in a transmission electron microscope. As controls, lesional skin samles from lamellar ichthyosis patients with transglutaminase 1 gene mutations (Akiyama *et al.*, 2001) or *ABCA12* mutations were also studied.

Cell culture

A skin sample from the patient was processed for primary keratinocyte culture, and cells were grown according to standard procedures in defined keratinocyte serum-free medium (Invitrogen Corp., Carlsbad, CA). After several passages in low-Ca^{2+} (0.09 mM) conditions, cultures were grown in high-Ca^{2+} (2.0 mM) conditions.

Antibodies

Polyclonal anti-ABCA12 antiserum was raised in rabbits using a 14 amino-acid sequence synthetic peptide (residues 2567–2580) derived from the ABCA12 sequence (NM 173076) as the immunogen (Akiyama *et al.*, 2005). The other primary antibody was mouse monoclonal anti-glucosylceramide antibody (Alexis Biochemicals, Lausanne, Switzerland).

Immunofluorescent labeling

Immunofluorescent labeling was performed as previously described (Akiyama *et al.*, 2000). Briefly, 6-μm-thick sections of fresh patient's skin was cut using a cryostat. The sections were incubated in primary antibody solution for 1 hour at 37°C. Antibody dilutions were as follows; 1/10 for anti-ABCA12 antiserum and 1/10 for anti-glucosylceramide antibody. The sections were then incubated in FITC-conjugated to rabbit anti-mouse Igs and tetramethylrhodamine isothiocyanate-conjugated goat anti-rabbit Igs diluted 1:100 (DAKO, Glostrup, Denmark) for 30 minutes at room temperature, followed by nuclear counterstain by TO-PRO-3 (Invitrogen, Carlsbad, CA). The sections were extensively washed with phosphate-buffered saline between incubations. The stained sections were then mounted with a cover slip and observed using a confocal laser scanning microscope.

CONFLICT OF INTEREST
The authors state no conflict of interest.

ACKNOWLEDGMENTS
We thank Ms Megumi Sato, Ms Maki Goto and Ms Akari Nagasaki for their fine technical assistance on this project. This work was supported in part by Grant-in-Aid from the Ministry of Education, Science, Sports, and Culture of Japan to M. Akiyama (Kiban B 16390312).

REFERENCES

Akiyama M (1999) The pathogenesis of severe congenital ichthyosis of the neonate. *J Dermatol Sci* 21:96–104

Akiyama M (in press a) Pathomechanisms of harlequin ichthyosis and ABC transporters in human diseases. *Arch Dermatol*

Akiyama M (in press b) Harlequin ichthyosis and other autosomal recessive congenital ichthyoses: the underlying genetic defects and pathomechanisms. *J Dermatol Sci*

Akiyama M, Sawamura D, Nomura Y, Sugawara M, Shimizu H (2003) Truncation of CGI-58 protein causes malformation of lamellar granules resulting in ichthyosis in Dorfman–Chanarin syndrome. *J Invest Dermatol* 121:1029–34

Akiyama M, Sugiyama-Nakagiri Y, Sakai K, McMillan JR, Goto M, Arita K *et al.* (2005) Mutations in ABCA12 in harlequin ichthyosis and functional rescue by corrective gene transfer. *J Clin Invest* 115:1777–84

Akiyama M, Smith LT, Shimizu H (2000) Changing patterns of localization of putative stem cells in developing human hair follicles. *J Invest Dermatol* 114:321–7

Akiyama M, Takizawa Y, Suzuki Y, Ishiko A, Matsuo I, Shimizu H (2001) Compound heterozygous TGM1 mutations including a novel missense mutation L204Q in a mild form of lamellar ichthyosis. *J Invest Dermatol* 116:992–5

Allikmets R, Gerrard B, Hutchinson A, Dean M (1996) Characterization of the human ABC superfamily: isolation and mapping of 21 new genes using the expressed sequence tags database. *Hum Mol Genet* 5:1649–55

Allikmets R, Singh N, Sun H, Shroyer NF, Hutchinson A, Chidambaram A *et al.* (1997a) A photoreceptor cell-specific ATP-binding transporter gene (ABCR) is mutated in recessive Stargardt macular dystrophy. *Nat Genet* 15:236–46

Allikmets R, Shroyer NF, Singh N, Seddon JM, Lewis RA, Bernstein PS *et al.* (1997b) Mutation of the Stargardt disease gene (ABCR) in age-related macular degeneration. *Science* 277:1805–7

Annilo T, Shulenin S, Chen ZQ, Arnould I, Prades C, Lemoine C *et al.* (2002) Identification and characterization of a novel ABCA subfamily member, ABCA12, located in the lamellar ichthyosis region on 2q34. *Cytogenet Genome Res* 98:169–76

Borst P, Elferink RO (2002) Mammalian ABC transporters in health and disease. *Annu Rev Biochem* 71:537–92

Brooks-Wilson A, Marcil M, Clee SM, Zhang LH, Roomp K, van Dam M *et al.* (1999) Mutations in ABC1 in Tangier disease and familial high-density lipoprotein deficiency. *Nat Genet* 22:336–45

Dean M, Rzhetsky A, Allikmets R (2001) The human ATP-binding cassette (ABC) transporter superfamily. *Genome Res* 11:1156–66

Hayden MR, Clee SM, Brooks-Wilson A, Genest J Jr, Attie A, Kastelein JJ (2000) Cholesterol efflux regulatory protein, Tangier disease and familial high-density lipoprotein deficiency. *Curr Opin Lipidol* 11:117–22

Higgins CF (1992) ABC transporters: from microorganisms to man. *Annu Rev Cell Biol* 8:67–113

Holleran WM, Takagi Y, Menon GK, Legler G, Feingold KR, Elias PM (1993) Processing of epidermal glucosylceramides is required for optimal mammalian cutaneous permeability barrier function. *J Clin Invest* 91:1656–64

Ishida-Yamamoto A, Simon M, Kishibe M, Miyauchi Y, Takahashi H, Yoshida S *et al.* (2004) Epidermal lamellar granules transport different cargoes as distinct aggregates. *J Invest Dermatol* 122:1137–44

Judge MR, McLean WHI, Munro CS (2004) Disorders of keratinization. In: *Rook/Wilkinson/Ebling: Textbook of Dematology.* (Burns T, Breathnach S, Cox N, Griffiths C, eds), Oxford, UK: Blackwell Science, 34.1–11

Kelsell DP, Norgett EE, Unsworth H, The M-T, Cullup T, Mein CA *et al.* (2005) Mutations in ABCA12 underlie the severe congenital skin disease harlequin ichthyosis. *Am J Hum Genet* 76:794–803

Klein I, Sarkadi B, Varadi A (1999) An inventory of the human ABC proteins. *Biochim Biophys Acta* 1461:237–62

Lefèvre C, Audebert S, Jobard F, Bouadjar B, Lakhdar H, Boughdene-Stambouli O *et al.* (2003) Mutations in the transporter ABCA12 are associated with lamellar ichthyosis type 2. *Hum Mol Genet* 12:2369–78

Lefèvre C, Bouadjar B, Ferrand V, Tadini G, Mégarbané A, Lathrop M *et al.* (2006) Mutations in a new cytochrome P450 gene in lamellar ichthyosis type 3. *Hum Mol Genet* 15:767–76

Oram JF (2002) Molecular basis of cholesterol homeostasis: lessons from Tangier disease and ABCA1. *Trends Mol Med* 8:168–73

Orso E, Broccardo C, Kaminski WE, Bottcher A, Liebisch G, Drobnik W *et al.* (2000) Transport of lipids from Golgi to plasma membrane is defective in tangier disease patients and Abc1-deficient mice. *Nat Genet* 24:192–6

Peelman F, Labeur C, Vanloo B, Roosbeek S, Devaud C, Duverger N *et al.* (2003) Characterization of the ABCA transporter subfamily: identification of prokaryotic and eukaryotic members, phylogeny and topology. *J Mol Biol* 325:259–74

Rust S, Rosier M, Funke H, Real J, Amoura Z, Piette JC *et al.* (1999) Tangier disease is caused by mutations in the gene encoding ATP-binding cassette transporter 1. *Nat Genet* 22:352–5

Schmitz G, Langmann T (2001) Structure, function and regulation of the ABC1 gene product. *Curr Opin Lipidol* 12:129–40

Shibaki A, Akiyama M, Shimizu H (2004) Novel ALDH3A2 heterozygous mutations are associated with defective lamellar granule formation in a Japanese family of Sjögren–Larsson syndrome. *J Invest Dermatol* 123: 1197–9

Uitto J (2005) The gene family of ABC transporters – novel mutations, new phenotypes. *Trends Mol Med* 11:341–3

Vielhaber G, Pfeiffer S, Brade L, Lindner B, Goldmann T, Vollmer E *et al.* (2001) Localization of ceramide and glucosylceramide in human epidermis by immunogold electron microscopy. *J Invest Dermatol* 117: 1126–36

Weng J, Mata NL, Azarian SM, Tzekov RT, Birch DG, Travis GH (1999) Insights into the function of Rim protein in photoreceptors and etiology of Stargardt's disease from the phenotype in abcr knockout mice. *Cell* 98: 13–23

Williams ML, Elias PM (1987) Genetically transmitted, generalized disorders of cornification; the ichthyoses. *Dermatol Clin* 5:155–78

Volume 54(1): 109–118, 2006
Journal of Histochemistry & Cytochemistry
http://www.jhc.org

ARTICLE

Colocalization of Multiple Laminin Isoforms Predominantly beneath Hemidesmosomes in the Upper Lamina Densa of the Epidermal Basement Membrane

James R. McMillan, Masashi Akiyama, Hideki Nakamura, and Hiroshi Shimizu

Creative Research Initiative Sousei (JRM) and Department of Dermatology, Graduate School of Medicine (JRM,MA,HN,HS), Hokkaido University, Sapporo, Japan

SUMMARY Multiple laminin isoforms including laminins 5 (α3 β3 γ2), 6 (α3 β1 γ1), 10 (α5 β1 γ1), and possibly laminins 7 (α3 β2 γ1) and 11 (α5 β2 γ1) are present in the epidermal basement membrane. However, only the precise epidermal ultrastructural localization of laminin 5 (α3 β3 γ2) has been elucidated. We therefore determined the precise expression and ultrastructural localization of the α5, β1, β2, and γ1 chains in the epidermis. The expression of laminin chains in skin samples was analyzed from patients with epidermolysis bullosa (EB, n=15) that harbor defects in specific hemidesmosome (HD)-associated components. The expression of the α5, β1, and γ1 chains (present in laminins 10/11) and β2 chain (laminins 7/11) was unaffected in all intact (unseparated) skin of EB patients including Herlitz junctional EB with laminin-5 defects (n=6). In the basement membrane of human epidermis, the α5, β1, β2, and γ1 chains were expressed but also localized to the dermal vessels. Immunogold electron microscopy of normal human epidermis localized the α5, β1, β2, and γ1 chains to the upper lamina densa, with between 84% and 92% of labeling restricted to beneath the HDs, similar to laminin 5 (n≥200 gold particles per sample, sample number n=4) but distinct from collagen IV labeling (with only 63% labeling beneath HDs, p<0.001). Taken together, the majority of the α5β1/β2γ1 laminin chains are located beneath HDs. This suggests that laminin-10-associated chains have specific functions or molecular interactions beneath HDs in the epidermal basement membrane.

(J Histochem Cytochem 54:109–118, 2006)

KEY WORDS
anchoring filament
epidermal basement membrane
hemidesmosome
immunoelectron microscopy
laminin 5
laminin 10

IN SKIN, laminins are present in the epidermal basement membrane, around blood vessels, nerves, and adnexal structures. It is generally thought that laminin 5 (α3 β3 γ2), possibly laminin 6 (α3 β1 γ1), and laminin 10 (α5 β1 γ1) are expressed in the human epidermal basement membrane (Aumailley and Rousselle 1999) (see Figure 1). The expression of laminins 7 (α3 β2 γ1) and 11 (α5 β2 γ1) has yet to be confirmed in the adult human epidermis (Aumailley and Rousselle 1999). Of these, laminin 5 (α3 β3 γ2) is the most well-studied epidermal isoform (Nishiyama et al. 2000; Mercurio et al. 2001; Geuijen and Sonnenberg 2002; McMillan et al. 2003b). Laminin 5 is thought to be crucial for the correct assembly and adhesion of hemidesmosomes (HDs) via the receptor, the α6β4 integrin (Niessen et al. 1994).

The distinct roles of laminin isoforms in the processes of cutaneous morphogenesis are poorly understood. Laminin 10 (α5 β1 γ1), however, has recently been implicated in several functions including hair follicle development (Li et al. 2003). In an α5 chain (laminin 10/11) knockout mouse model, the addition of exogenous laminin 10 was used to correct follicular development (Li et al. 2003). Laminin 10 is therefore implicated in hair follicle cell growth and adhesion (Gu et al. 2001; Pouliot et al. 2002; Li et al. 2003). Cell adhesion assays have demonstrated that multiple laminins (including laminins 5, 10, and 11) can act as adhesive substrates for keratinocytes and that this adhesion is mediated by the integrins α3β1 and α6β4

Correspondence to: James R. McMillan, MSc, PhD, Department of Dermatology, Hokkaido University Graduate School of Medicine, Kita-ku, Sapporo, 060-8638, Japan. E-mail: jrm57@med.hokudai.ac.jp

Received for publication March 28, 2005; accepted September 6, 2005 [DOI: 10.1369/jhc.5A6701.2005].

 0022-1554/05/$3.30

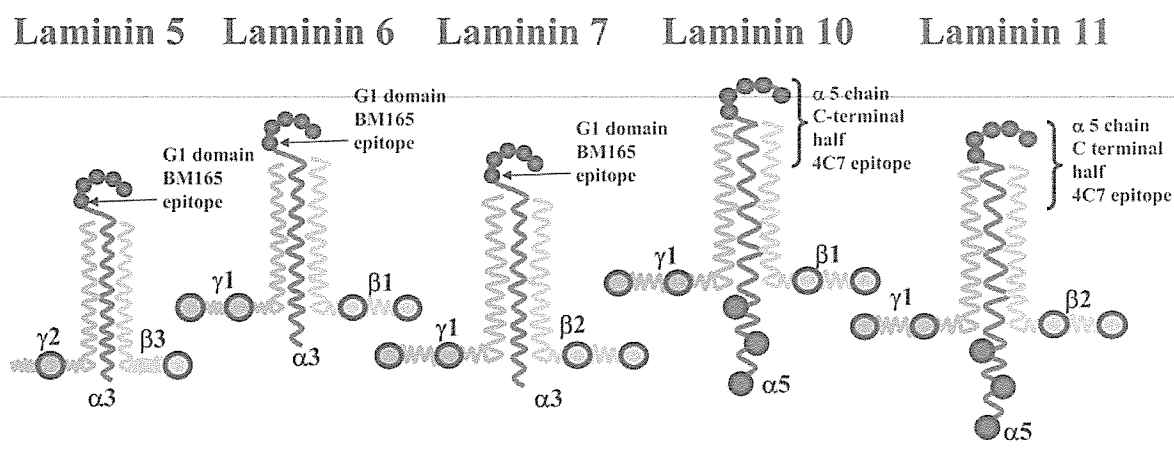

Figure 1 Schematic diagram showing the structure of laminin 5 and 10 chains and the position of two antibody binding sites in the α3 chain G1 domain (BM165) and the carboxyl terminal half of the α5 chain (4C7). This schematic diagram is not drawn to scale and does not include any α3 chain splice variants of laminin 5 (α3 β3 γ2). The antibody BM165 binds to the first globular (G1) domain of the α3 chain of laminins 5/6 (McMillan et al. 2003b), whereas the antibody 4C7 binds to the carboxyl terminal half end of the α5 chain (present in both laminins 10 and 11).

(Pouliot et al. 2002). However, in certain non-epithelial cells, the integrins α3β1, α6β1, and α6β4 and α dystroglycan are expressed and have been identified as possible laminin 10/11 receptors (Kikkawa et al. 1998, 2000; Yu and Talts 2003).

Antibodies are now available that recognize specific laminin chains and provide new tools to investigate the structure of the epidermal basement membrane. These antibodies include 4C7 (Engvall et al. 1990; Tiger et al. 1997) that recognizes a carboxyl terminal domain of the human α5 chain of laminins 10 (α5 β1 γ1, see Figure 1) and 11 (α5 β2 γ1). This antibody blocks the epitope involved in neurite cell adhesion to the laminin α5 chain (Engvall et al. 1986; Makino et al. 2002). Further laminin-specific antibodies to β and γ chains include 2E8 (recognizing the β1 chain (Engvall et al. 1986), D18 (γ1) (Sanes et al. 1990), and C4 (β2) (Hunter et al. 1989).

To better understand the position and possible functions of epidermal molecules, we examined the precise localization of the α5, β1, β2, and γ1 laminin chains and collagen IV in the interfollicular and follicular epidermal basement membrane. In addition, the expression of laminin chains was also assessed in a range of epidermolysis bullosa (EB) patients' skin harboring defects in several basement membrane components, including laminin 5. We have quantitatively analyzed and compared the localizations of laminin α5, β1, β2, and γ1 chains with that of laminin 5 (α3 β3 γ2) from our previously published data (McMillan et al. 2003b) and collagen IV. Comparison of α5, β1, β2, and γ1 chain expression with laminin 5, a well-studied HD-associated isoform, will determine a more precise localization for these laminin isoforms. Our data support the hypothesis that multiple laminin isoforms colocalize beneath HDs in normal and diseased epidermal basement membranes.

Materials and Methods

Skin Samples

Samples of adult and neonatal control skin from non-specialized sites (abdomen, arm, thigh, $n=8$; and scalp skin, $n=2$) were obtained from routine surgical procedures. Skin samples were frozen for cryostat sectioning or processed for post-embedding immunogold electron microscopy (IEM) as described below. In all cases, the biopsies were performed with the patient's or guardian's informed consent, with the relevant institutional approval for experiments handling human material, and in accordance with the Helsinki Declaration.

Skin samples from patients affected with a group of rare genodermatoses, EB, were included in this study ($n=15$, see Table 1). Details of the number of patients for each EB disease subtype, their age at biopsy, details of any identified mutations, or significant results of diagnostic antibody staining are listed, in addition to the results of their laminin antibody staining findings (see Table 1). Four Herlitz junctional (HJ) EB patients harbored laminin-5 chain mutations that were reported in the literature (Takizawa et al. 1998a–d). In one EB simplex associated with muscular dystrophy (EBS-MD) patient, genetic defects have been reported (Pulkkinen et al. 1996).

Confocal Immunofluorescence Microscopy

Indirect immunofluorescence was performed as previously described (Kennedy et al. 1985) using cryostat skin sections. Laminin chain expression was confirmed in control skin using the following antibodies: 4C7 recognizing the human α5 chain (see Figure 1) present in laminins 10 and 11 (dilution

Table 1 Comparison of laminin 5 and laminin 10 expression in patients with various forms of epidermolysis bullosa

EB disease subtype	Deficient protein	Patients' sex, age, mutation, and staining details	Laminin-5 γ3 chain GB3 expression	Laminin-10 α5 chain 4C7 expression
Control (5)	Normal	M/31 years, 33 years, 41 years, 45 years, F/15 years	+++	+++
HJEB (6)	Laminin 5	M/1 month, W610X/Q166X LAMB3	–	+/++
		F/9 months, 1997-2A>C (homozygous, LAMB3)		
		F/1 month, Q936X LAMB3		
		M/1 month, 1929delCA/W610X LAMB3		
		F/2 months, M/1 month, laminin-5 negative (GB3 moAb)		
NHJEB (2)	Laminin 5	M/12 years, M/5 years, laminin-5 reduced (GB3 moAb)	+	+++
NHJEB (2)	Collagen XVII	M/21 years, F/35 years, G252X collagen XVII negative (233, 1A8C moAb)	+++	+++
SRDEB (2)	Collagen VII	M/7 years, M/1 year, collagen VII negative (LH7:2 moAb)	+++	+++
JEB-PA/PA-EBS (1)	Integrin α6β4	F/1 month, α6β4 integrin negative (3E1,GOH3 moAb)	+++	+++
EBS-MD (2)	Plectin	M/27 years, M/9 years, plectin negative (HD1-121 moAb)	+++	+++

EB, epidermolysis bullosa; HJEB, Herlitz junction epidermolysis bullosa; NHJEB, non-Herlitz junctional epidermolysis bullosa; SRDEB, severe recessive dystrophic epidermolysis bullosa; JEB-PA, junctional epidermolysis bullosa associated with pyloric atresia; which is also known as EBS-PA, epidermolysis bullosa associated with pyloric atresia. +++, normal, bright staining pattern along dermal–epidermal junction; ++, reduced dermal–epidermal junction staining compared to controls; +, severely reduced dermal–epidermal junction staining compared to controls; –, absent dermal–epidermal junction staining compared to controls.

1:25; Chemicon International, Temecula, CA) (Engvall et al. 1990; Tiger et al. 1997). The monoclonal antibody 2E8 recognizing the β1 chain (neat) (Engvall et al. 1986), the monoclonal antibody D18 that recognizes the γ1 chain (see Figure 1) (neat) (Sanes et al. 1990), and an antibody C4 to the β2 chain (see Figure 1) (used neat) (Hunter et al. 1989) were also included. The antibodies 2E8, D18, and C4 were obtained from the Developmental Studies Hybridoma Bank, University of Iowa (Iowa City, IA). The mouse monoclonal M3F7 recognizing the helical domain of the α1 and α2 chains of collagen IV (used neat) (Foellmer et al. 1983) was also obtained from the Developmental Studies Hybridoma Bank. Laminin-5 antibodies included the mouse monoclonal BM165 directed against the laminin-5 α3 chain terminal first globular (G1) domain (see Figure 1) (diluted 1:50) (Marinkovich MP, unpublished data) (McMillan et al. 2003b); K140 directed against the laminin-5 β3 chain adjacent to domain IV; GB3 directed against the laminin-5 γ2 chain (Harlan Sera Lab; Loughborough, UK); and a rabbit polyclonal serum directed against the entire laminin-5 molecule (1:200) (McMillan et al. 2003b). The melanocyte marker antibody TMH-1 recognized the b-locus protein (rat antibody, 1:10 dilution) and was previously described by Masunaga et al. (1996).

Epidermal sections were fixed in cold acetone (−20C) for 10 min and incubated with 5% normal rabbit sera in 0.1 M Dulbecco's PBS for 5 min at 37C. Sections were incubated with primary antibodies and subsequently with secondary antibodies conjugated to fluorescein isothiocyanate or Texas Red (FITC; rabbit anti-mouse IgG or goat anti-rabbit IgG, 1:200; DAKO, Tokyo, Japan; Texas Red conjugated donkey anti-rabbit; Amersham, UK). To label TMH-1, a preabsorbed cyanine (CY5)-conjugated goat anti-rat antibody was used (Jackson ImmunoResearch; West Grove, PA). All secondary antibodies were diluted in 3% BSA in 0.1 M PBS for 30 min at 37C in a darkened, humidified chamber. Sections were then labeled with a ToPro-3 nuclear counterstain (diluted 1:20,000, blue channel; Jackson ImmunoResearch) if appropriate. The sections were then mounted in Permafluor (Thermo Shandon; Pittsburgh, PA) and examined with a confocal microscope (Fluoview FV300; Olympus, Tokyo, Japan) using an inverted microscope (IX70; Olympus). Controls included normal skin cryostat sections with the primary antibody substituted by PBS, myeloma supernatant, or an irrelevant immunoglobulin isotype, as a negative control. All experiments were performed at least in duplicate.

Immunogold Electron Microscopy

Four samples of human skin were cryofixed and processed for postembedding IEM according to the previously described methods (Shimizu et al. 1989,1990). Samples were washed in PBS and cryoprotected in 20% glycerol (in PBS) for up to 1 hr at 4C. Subsequently, cryofixation was performed in liquid propane at −190C using a freeze plunge apparatus (Leica CPC; Cambridge, UK) followed by freeze substitution over 3 days at −80C in methanol using an automated freeze substitution system (AFS; Leica). Specimens were embedded in Lowicryl K11M (Ladd Research Industries; Burlington, VT) resin over 4 days at −60C. The temperature was gradually raised and the resin was polymerized under UV light and liquid nitrogen vapor at 10C. Ultrathin sections were then cut and collected on pioloform-coated nickel grids. Sections were stained with uranyl acetate only (15 min) and observed with a transmission electron microscope (Hitachi H-7100; Tokyo, Japan) at 75 kV. Blocks showing good ultrastructure were selected for immunolabeling experiments. Sections were preincubated in buffer containing PBS with 5% normal goat serum (NGS), 1% BSA, and 0.1% gelatin. Primary antibodies or human antisera were all diluted in PBS buffer containing 1% NGS, 1% BSA, and 0.1% gelatin and incubated at 37C for 2 hr. The sections were then washed in a drop of PBS buffer four times (5 min each) and placed on a drop of secondary linker antibody, again diluted in PBS buffer (for 2 hr at 37C). The secondary antiserum, rabbit anti-mouse IgG (DAKO; Ely, UK) was diluted 1:500. Sections were then incubated with a final antibody layer using 5-nm gold-conjugated labeled goat anti-rabbit or goat anti-mouse antibodies (Biocell; Cardiff, UK) diluted 1:500 in Tris-buffered saline (TBS) for 2 hr at 37C. For double labeling on K11M sections, the α5 chain of laminins 10/11 (4C7 and a 5-nm

gold-conjugated goat anti-mouse) and rabbit anti-laminin 5 (polyclonal highlighted by 15-nm gold-conjugated goat anti-rabbit; Biocell) were used. Sections were washed twice in TBS buffer and twice in distilled water (5 min each). After staining with 15% alcoholic uranyl acetate (3 min) and lead citrate (15 min), sections were observed with a transmission electron microscope (H-7100; Hitachi). Controls included normal skin sections with the primary antibody substituted by PBS, myeloma supernatant, preimmune rabbit serum, or an irrelevant immunoglobulin isotype, as a negative control. All experiments were performed in triplicate.

Immunogold Quantitative Analysis

The techniques for ultrastructural labeling were similar to those performed by McMillan et al. (2003b). Electron micrographs were taken at a standard magnification (30K) and were enlarged by a standard factor ×2.08. The final magnification (×62,500) was checked using electron micrographs taken of a carbon diffraction grating. For standardization purposes, all observations were made by one observer (JRM). At least 200 gold particles were assessed per specimen for each antibody or antiserum and four specimens from different individuals were examined (see Table 1 and Table 2). A 5-nm immunogold-conjugated final antibody layer was used. The percentage of gold particles perpendicularly beneath an observable electron-dense HD cytoplasmic outer attachment plaque as described by McMillan and Eady (1996) was scored and calculated from a large number of gold particles in skin from four individuals.

Only non-obliquely sectioned areas of dermal–epidermal junction were included with clearly defined HD plaques, lamina lucida (LL), and lamina densa (LD). The dermal–epidermal junction beneath melanocytes or in damaged areas was excluded from this study. Gold particles that appeared clumped or associated with any deposit were excluded.

For each antibody or antisera, the positions of gold particles were statistically tested by one-way ANOVA and a two-sample *t*-test using the Minitab statistical package (Minitab Inc; University of Pennsylvania, Philadelphia, PA). An antibody (4C7) that recognizes a carboxyl terminal domain of the α5 chain of laminins 10/11 was used to determine the mean position of labeling directly beneath the keratinocyte plasma membrane (Engvall et al. 1986; Makino et al. 2002)(see Figure 1 for epitope position). The labeling of the α5 chain was compared with the distribution of the G1 domain of laminin-5 α3 chain (using data previously reported by McMillan et al. 2003b).

Results

Confocal Fluorescence Microscopy of Control Skin

Laminin-5 staining was restricted to the dermal–epidermal junction in control skin (data not shown). This was similar to the dermal–epidermal junction staining of α5 chain of laminins 10 (data not shown). Laminins 10 and 11 were also expressed in dermal blood vessels. Laminin 11 (as identified by the β2 chain) dermal–epidermal junction staining was present in adult control thigh and arm skin but was variable in other samples including scalp skin. Therefore, β2 chain expression appears to be distinct and independent from that of the α5 chain. Staining for the α5, β1, and γ1 chains was weaker in the adult dermal–epidermal junction than in blood vessels (data not shown), whereas dermal–epidermal junction staining was generally brighter in younger skin samples (<16 years, data not shown). This would appear to support a previous report of age-dependent expression of the laminin 10/11 chains (Pouliot et al. 2002).

Confocal fluorescence microscopy (Figures 2A–2C) showed that both laminin-5 and α5 chains are expressed in the dermal–epidermal junction of control interfollicular epidermis except for small gaps (white arrows in Figures 2A and 2B) beneath small isolated cells presumed to be melanocytes staining blue for the melanocyte marker, TMH-1 (Figures 2A and 2B) (Masunaga et al. 1996). These data suggest that laminin-10 chains are restricted to beneath keratinocytes and are not expressed beneath melanocytes.

A previous scalp skin and hair follicle immunohistochemical study (Akiyama et al. 1995) demonstrated a specific staining pattern for many HD and anchoring filament components, particularly laminin 5, which manifests as reduced staining around the lower hair bulb and a reemergence of staining over the dermal papilla region (Akiyama et al. 1995). We observed this

Table 2 Immunogold particle distribution shows the majority of laminin labeling is restricted to beneath the hemidesmosome (HD) plaque

Antibody/antisera	Recognizes chain and epitope	Present in which chain/isoform(s)	Number of skin samples	Frequency of gold particles under HDs % (±SD)
Laminin 5	All chains[a]	Lam 5[a]	2[a]	77–88[a]
BM-165	α3 chain	Lam 5/6	4	82.65 (±3.87)
4C7	α5 chain	Lam 10/11	4	84.3 (±3.89)
2E8	β1 chain	Lam 6/10	4	91.7 (±3.99)
C4	β2 chain	Lam 7/11	4	88.4 (±3.56)
D18	γ1 chain	Lam 6/7/10/11	4	92.0 (±2.65)
M3F7	Collagen IV	α1/α2 helical (IV)	4	61.3 (±3.05)

[a]Data from McMillan et al. 2003b and Masunaga et al. 1996.